THE STUDY ON THE INTERPLAY OF SUPERCONDUCTIVITY AND MAGNETISM IN IRON BASED SUPERCONDUCTORS

By

Mesfin Asfaw Afrassa

A DISSERTATION SUBMITTED TO

THE DEPARTMENT OF PHYSICS

ADDIS ABABA UNIVERSITY

IN FULFILLMENT OF THE REQUIREMENTS

FOR THE DEGREE OF

DOCTOR OF PHILOSOPHY in PHYSICS

ADDIS ABABA, ETHIOPIA

APRIL 2016

ADDIS ABABA UNIVERSITY

SCHOOL OF GRADUATE STUDIES

This is to certify that the dissertation prepared by **Mesfin Asfaw Afrassa**, entitled "**The Study on the Interplay of Superconductivity and Magnetism in Iron based Superconductors**" and submitted in fulfillment of the requirements for the degree of **Doctor of Philosophy**(Physics) complies with the regulations of the university and meets the accepted standards with respect to originality and quality.

Dated: April 2016

Signed by the Examining Committee:

External Examiner: _____
Dr. Maria Elena Bascones

Internal Examiner: _____
Dr. Cherinet Amente

Research Supervisors: _____
Professor P. Singh

Chair person of the department: _____
Dr. Teshome Senbeta

Table of Contents

List of Figures

Acknowledgements

First and for most, I would like to thank my supervisor professor P.Singh, for his support through out my study. I would like to thank professor B. Buchner and Dr Anja U. B. Wolter, for their permission and support to use SQUID and other facilities in IFW Dresden, Germany. I would further thank Dr Fabio(University of Cagliari, Italy) who introduced me Quantum Espresso.
I acknowledge the financial support of Addis Ababa University Graduate office, IFW Dresden, Adama Science and Technology University, and DREAM ACP project.
I am grateful to Dr Teshome, chairman of the department, w/r Tsilate, secretary of the department, Dr Lemi and Dr Belayneh, the former chairman of the department of Physics, AAU, for their help through out my contact with the department. I appreciate the support from the staff at AAU and ASTU. I would like to thank every one in particular, Tesfaye M., Sintayehu M., Lata G., Girma K., Gezahegn A., Kinde Y., Gashaw B. ,Kelbesa, Giulia M., Markus, Sebastian, Tomazo and others, for their support while I was a graduate student.
Finally, I would like to express thanks from bottom of my heart to all my family members, in particular, Genet, Maya and Hable for their love, and continues support. On the top I thank the Almighty God.
Mesfin A. A
Addis Ababa University
April, 2016

General Abstract

The study on the interplay of Superconductivity(SC) and Magnetism has attracted much interest on iron based superconductors following the report on $LaFeAsO_{0.89}F_{0.11}$ to unravel the basic mechanism in high temperature superconductors(HTC). In this dissertation we study the properties of the so called 1111-family of iron based superconductors applying different techniques including, Greens function formalism, magnetization measurement using VSM-SQUID, and DFT as implemented in QE and Fleur code.

The first part of this work (chapter 3) consists of theoretical calculations applying double time temperature dependent Green function techniques. Starting with a model Hamiltonian consisting of a pairing interaction, magnetic interactions of Heisenberg type by local electrons and an interaction of itinerant electrons with localized electrons, we determined the expression for the superconducting transition temperature, T_C. The expressions indicate that magnetization suppresses Superconductivity, and there might be a coexistence below critical temperature. The result is in broad agreement with experimental findings.

In the second part (chapter 4), a magnetization measurement with VSM SQUID on three site doped, $La_{1-x}Y_xFe_{1-y}Mn_yAsO_{0.89}F_{0.11}$, samples was done, where the effects of Mn doping on Fe site and Y doping on La site in $LaFeAsO_{1-x}F_x$ simultaneously studied, and hence the superconducting critical temperature Tc of different samples was determined. Our results indicate that Y doping has a stabilizing effect on Superconductivity even in the presence of Mn doping. Mn has a pair breaking effect even a small amount of it suppresses T_C.

Finally, computational work applying the DFT in first principle method as implemented in QE and Fleur code is done(chapter 5). Since iron based superconductors have multi-band character in their electronic structure, we were interested to see the effect of substitution in the band structure and Fermi surface and in turn the effect on T_C. The result on the band structures show that Ru substitution changes the hole bands and not the electron bands. One of the possible reason is perhaps that Ru substitution does not induce additional electrons, which is in agreement with NMR and resistivity measurement report. Fermi surfaces (FS) of SmFeAsO show that at Ru = 0.25 it has

a suppressing effect and at Ru = 0.50 a favoring effect on superconductivity. It is predicted that higher T_C can be achieved at Ru = 0.50 substitution for $SmFeAsO_{0.85}F_{0.15}$, in case nesting is an indication for Superconductivity. Calculations indicates that superconductivity can be achieved only for a strong paring potential, which can not be explained by BCS type pairing. Generally, Ru is understood to have effects on LaFeAsO and SmFeAsO compounds and one can not treat these systems with same existing theories.
keywords: Superconductivity (SC), Iron based Superconductors(IBS), Green Functions, Superconducting quantum interference device (SQUID), Quantum Espresso (QE), Density of state(DOS), Fermi surface (FS), Density functional theory (DFT)

Chapter 1

Introduction to Superconductivity and Magnetism

Overview

In this chapter a short introduction will be given to superconductivity in general and to the recently discovered pnictides superconductors in particular. Firstly, a short summery is given about the discovery of Superconductivity and important superconducting parameters including BCS theory. After reviewing the most important discoveries a short brief discussion is given about the current topics of research, Iron based superconductors. Finally Magnetic properties of Superconductors are summarized.

1.1 Superconductivity

From macroscopic point of view one can define Superconductivity as a phenomenon of zero resistance. It is one of the most fascinating phenomena in Condensed Matter Physics. The temperature below which the electrical resistance of materials goes to zero is called superconducting critical temperature(T_C)[1]. This phenomena was discovered in 1911 and till now it is not well understood specially in high temperature superconductors (HTC) and iron based superconductors.

Materials that show such novel properties are in general classified as Conventional and non-Conventional superconductors. For the conventional superconducting materials the main mechanism responsible for the superconducting pairing is electron-phonon interactions, which was explained by BCS theory. BCS theory was proposed by Bardeen, Cooper, and Schrieffer in 1957 and is the most successful theory to explain superconductivity in certain superconductors. The Superconducting critical temperature (T_C) of conventional superconductors is low compared to non-conventional ones. The mechanism responsible for the superconducting pairing of the non-conventional superconductors is still not well understood.

In 1986, Bednorz and Muller discovered a lanthanum-based cuprate perovskite material with T_C of 35K[2]. The highest T_C in this class by now is 164K. The mechanism of Superconductivity in this class of material is still not well understood. The discovery of this HTC made it clear that BCS theory should be improved or a new theoretical concept is required.

A new class of iron-based superconductors was introduced in 2008 by Hosono group, in a fluorine-doped at oxygen site of LaFeAsO[3]. This parent compound(LaFeAsO) is the best system to study the properties of superconductivity. In fact the parent compound LnFeAsO is not superconducting, rather it is an anti-ferromagnetic (AFM) semi-metal[4].

1.2 BCS theory and beyond

Bardeen, Cooper and Schriefe(BCS) theory is one of the bench mark theory for superconductivity. It is a microscopic theory of superconductivity and mainly based on the attractive interaction between electrons that form pairs called cooper pairs. The basic formalism is in terms of creation and annihilation operators of the single particle electronic states. The BCS model Hamiltonian of a simplified system is expressed as

$$H = \sum_{k,\sigma} \varepsilon_k - \sum_{k,k':|\varepsilon(k)|,|\varepsilon(k)|\leq h\omega_D} V_{kk'} \hat{c}^{\dagger}_{k\uparrow} \hat{c}^{\dagger}_{-k\downarrow} \hat{c}_{-k'\downarrow} \hat{c}_{k'\uparrow}. \tag{1.1}$$

Here $\hat{c}^{\dagger}_{k\sigma}(\hat{c}_{k\sigma})$ is the creation (annihilation) operator of an electron in momentum-state k and spin σ. $\varepsilon_k = \hbar^2 k^2/2m - E_F$, $V > 0$ for attractive interaction.

The superconducting critical temperature T_C and density of state relates by the following well known BCS formula:

$$K_B T_C = 1.4 E_D \exp(-1/N(o)V) \tag{1.2}$$

where K_B is Boltzman constant, E_D is the Debye cut-off energy, N(o) is the density of states at the Fermi level, and V is the pairing potential. The term $N(o)V = \lambda$ is the coupling parameter. In the weak coupling limit, where BCS theory is valid is, $\lambda << 1$.

A more general description were given by Eliashberg theory in 1960. Eliashberg theory has been used to describe superconducting properties of different compounds where the original BCS theory was not able to describe. BCS equation(eq 1.2) was transformed in more general form called McMillan equation[5]:

$$T_c = \frac{\theta_D}{1.45} exp[-\frac{1.04(1+\lambda)}{\lambda - \mu * (1 + 0.62\lambda)}]. \tag{1.3}$$

Lambda(λ) can represent different kind of cooper pairing.

BCS theory has a limitation in describing highly correlated system like Iron based superconductors and HTCs [20, 21].

1.3 Iron based superconductors

Iron-based superconductors are iron-containing chemical compounds. The study on the iron based superconductors has got a great attention following the report on $LaFeAsO_{1-x}F_x$ [3]. The highest superconducting critical temperature T_C reaches 56k [6] by replacing La with other rare earth elements Ce, Pr, Nd, Sm, and Gd. This class of material provides a large number of superconducting compounds that are grouped in general stoichiometry of LnFeAsO ("1111") family (eg. Ln = La), MFe_2As_2("122") family(eg. M = Ba), MFeAs ("111") Family (eg.M = Li), and FeM ("11") family (eg. M = Se)[7, 8, 9, 10]. Both families of iron pnictides have a quasi-two-dimensional (2D) tetragonal crystal structure.

Fig (1.1) shows crystal structure of the main families of pnictides.

The parent compound LaFeAsO contains FeAs layers sandwiched by LaO layers. Each FeAs layer consists of a square-lattice Fe plane with As atoms above

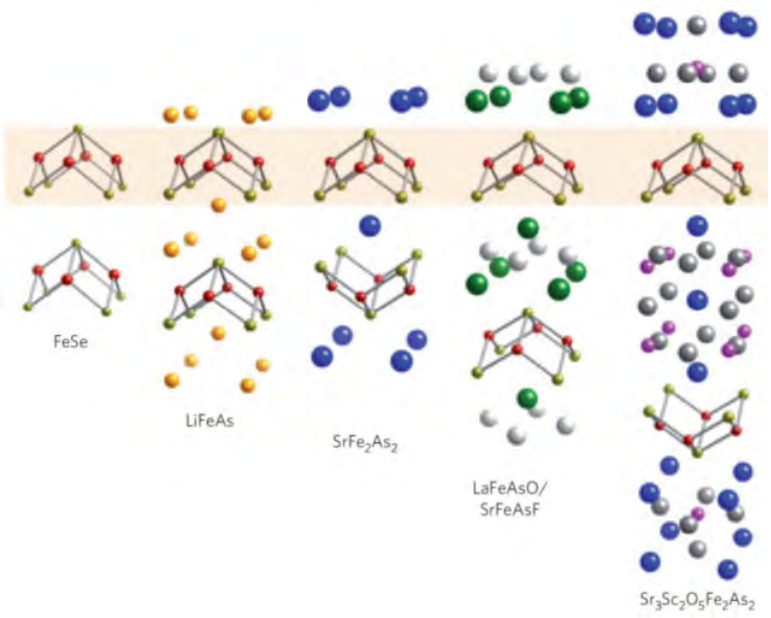

Figure 1.1: Crystal structures of some of iron-based superconductors(taken from Ref.[11]

Table 1.1: The maximum T_C for the main families of iron based superconductors yet found(taken from ref [12]).

Compounds	Familiy type	Maximum T_C
RFeAsO	1111	56K
AFe_2As_2	122	38K
LiFeAs	111	25K
FeSe	11	15K

and below the plane alternatively. The common feature of these main families of Iron based superconductors(the 1111, 122, 111, and 11 families of materials) is the presence of an identical FeAs (or FeSe) plane.

It was reported that these families of iron based superconductors attain different value of superconducting temperature T_C (table 1.1).

In many publications, much effort has been made theoretically and experimentally to identify the main cause of novel properties of materials. A deeper understanding on the doping effect of the electronic structure of this systems can provide insight into the interplay between magnetism and Superconductivity.

1.4 Magnetic properties

Superconductivity and Magnetisms are interrelated phenomena in high temperature superconductors. Meissner in 1933 discovered about the expulsion of a magnetic field when the superconductor is cooled below the superconductor's critical temperature. These materials called Type I, the induction B is given by

$$B = H + 4\pi M$$

where M is the magnetic moment per unit volume. A perfect diamagnetic has B = 0 inside, hence the volume susceptibility,

$$\chi = M/H = -1/4\pi.$$

There are materials called Type II where the magnetic field is not completely expelled (Fig 1.2). In the above expression, that relates the magnetic induction to the magnetic field in Gaussian units is in the absence of demagnetization effects.

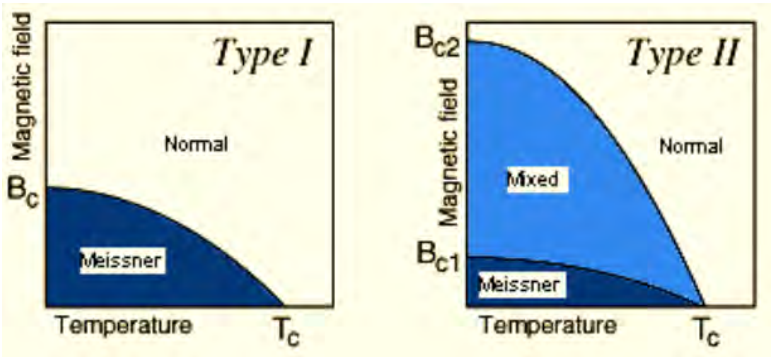

Figure 1.2: Phase diagrams of Type I and II superconductors

1.5 Magnetic Properties of Iron based superconductors (IBS)

After the discovery of high temperature superconductivity(HTC) in 1986, the study of magnetic properties has been an essential aspect of superconductivity.

Experimental and theoretical research has shown a significant progress on

the magnetic properties of iron based superconductors[15, 19] but not yet completely known. It is believed that understanding the interplay between Superconductivity and magnetism may lead to the possible mechanism for superconductivity.

Different experimental work on Ln1111 families of pnictides results with various phase diagrams. Fig (1.3) and Fig (1.4) show the phase diagrams of main families of iron based superconductors. It is known that a phase diagram provides an overview how the superconducting and magnetic properties are changed by external parameters. Until now it is not possible to express iron based superconductors in the same phase diagram.

The structural and magnetic transition up on doping was reported from different experimental techniques including, susceptibility and resistivity measurement, μSR, and x-ray diffraction.(ref. in [13]). For example, it was reported that the parent compound LaOFeAs shows a structural phase transition from a tetragonal symmetry to an orthorhombic and a magnetic phase transition to AFM SDW state at T_S = 156K and T_n = 138K respectively.

Electrons or holes doping suppresses the structure and/or the magnetic transition in favor of superconductivity. It is also observed that superconductivity and magnetism coexist in some compounds(Fig 1.4(a)). But still difficult to explain with the existing common theories.

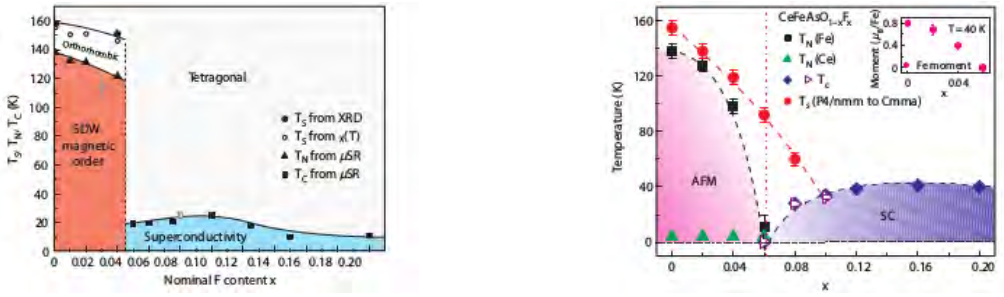

(a) $LaFeAsO_{1-x}F_x$ [16] (b) $CeFeAsO_{1-x}F_x$ [29]

Figure 1.3: Phase diagrams determined based on experimental data for $LaFeAsO_{1-x}F_x$, and $CeFeAsO_{1-x}F_x$

The study on the proximity of the magnetic and superconducting ground state is undergoing. In this line the importance of the magnetic and structural phases of these materials for superconductivity, and whether they coexist or compete is an important question to answer.

The other mysterious issue is the pairing mechanism in IBS. Theoretical [20]

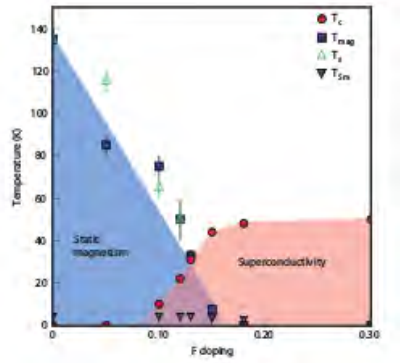

(a) $SmFeAsO_{1-x}F_x$ [17]

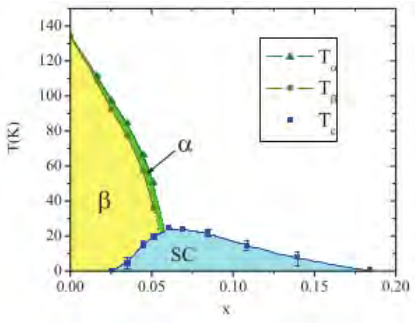

(b) $Ba(Fe_{1-x}Co_x)_2As_2$ [18]

Figure 1.4: Phase diagrams determined based on experimental data for $SmFeAsO_{1-x}F_x$, and $Ba(Fe_{1-x}Co_x)_2As_2$

and experimental[21] report depicts that Superconductivity in iron based superconductors,similarly to high-temperature copper based superconductor, is most likely not mediated by phonon coupling, but rather either by some magnetically mediated coupling or due to electron correlations.

1.6 Band structure, Fermi surfaces, and DOS of Iron based superconductors

Electronic band structure calculation has been popular after the discovery of DFT in 1960. It is one of the important parameter to study various properties of materials, such as electrical and structural.
Experimentally electronic band structure and Fermi surfaces can be determined by different techniques including Angle Resolved Photo Emission Spectroscopy(ARPES) and de Haas-Van Alphen(dHvA) effect.
First principal calculation also leads to obtain electronic band structure and Fermi surfaces. Figure 1.5 shows the band structure of undoped 1111(LaFeAsO) and undoped 122 ($BaFe_2As_2$), reproduced by the concept of non spin polarized calculation [22]. The lattice parameters were based on the experimental result. The result of the calculation shows that Fe 3d orbital bands are present near the Fermi energy. The figure also shows 5 bands are crossing the Fermi level, that depicts the multi band nature of the iron based compounds.
The Fermi surface (FS) in most pnictides includes electron-like cylinders in the corners of the Brillouin zone and the hole-like cylinders along the Γ-Z

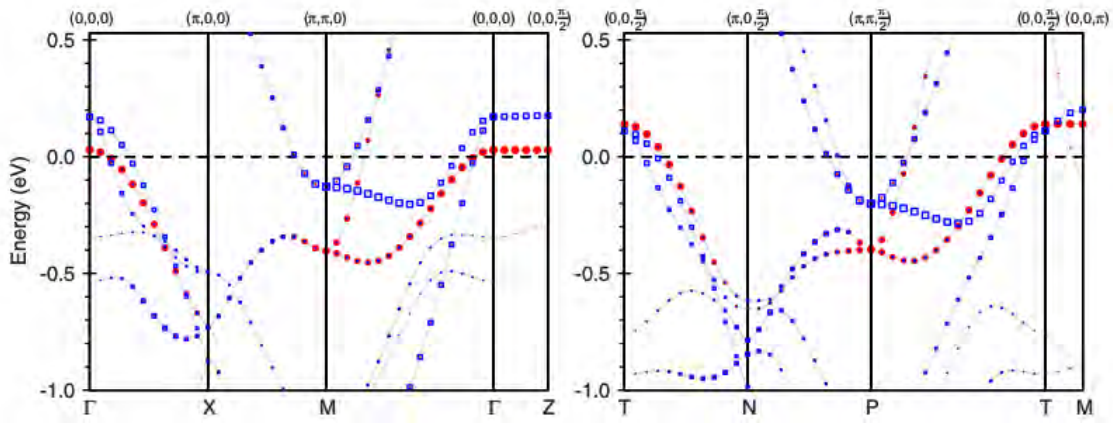

Figure 1.5: Band structure of LaFeAsO(left) and $BaFe_2As_2$(right)(taken from ref. [22])

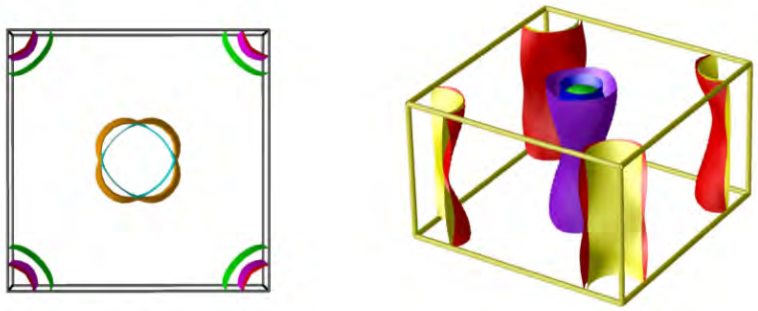

Figure 1.6: Fermi surfaces of LaFeAsO(left) and $BaFe_2As_2$(right)(taken from ref. [23])

line(Fig 1.6). But there is still a difference among the different families of iron based superconductors. For instance, the 1111-family undoped shows 2-dimensionality and the 122-family undoped one is 3-dimensional in character. Fig 1.6 shows the Fermi surfaces of non magnetic LaFeAsO and $BaFe_2As_2$ [23].

Density of State(DOS) in superconductivity is an important parameter to understand several properties. If the number of DOS near the Fermi level is changing, for instance by doping, then the properties of the material may change dramatically. Applying Density Functional theory as implemented in Quantum Espresso(QE) code one can calculate the DOS of a compounds up on substitution. Fig 1.7 is a typical example for DOS of LaOFeAs.

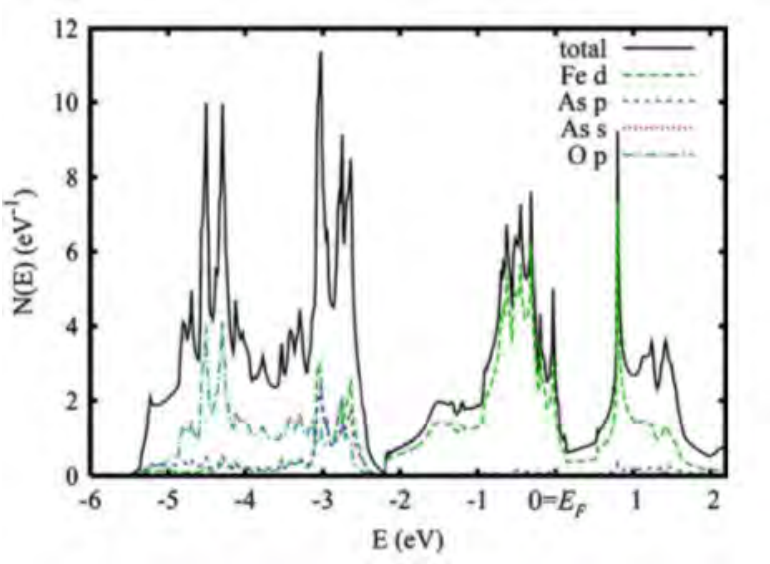

Figure 1.7: Calculated density of states in LaOFeAs (solid line) and partial contributions to it from the orbitals of Fe, As and O (dashed lines)[24]

Chapter 2

Methods

Overview

In this chapter a short introduction will be given to different methods used in this dissertation. Firstly, a short summery is given about Green Function and in particular Double - time Green Function. Secondly a short description about VSM-SQUID and the Physics of the instrument is given. Finally First principle method(DFT) is summarized.

2.1 Green Function

Green function is widely used in Condensed Matter Physics particularly to study the interactions of many body system [40, 41]. It is helpful to approximate a measurable physical quantities, like the expectation values and correlation function.

2.1.1 Double-time Green Functions

There are different types of Green functions. In this Section, we briefly review the double-time temperature-dependent Green functions . It was introduced by Bogoliubov and Tyablikov [42] and reviewed by Tyablikov [43].
Consider a many-particle system with the time-independent Hamiltonian $H = H_o - \mu N$; μ is the chemical potential, N is the operator of the total number of particles, and we have chosen our units so that $\hbar = 1$.
Let A(t) and B(t') be some operators, which can be expressed as the product of the quantized field operators . The time development of these operators in the Heisenberg representation is given by:

$$A(t) = exp(iHt)A(0)exp(-iHt) \tag{2.1}$$

We define three types of Green functions, the retarded, advanced, and causal Green functions:

$$G_r(t,t') \equiv \ll \hat{\mathbf{A}}(t); \hat{\mathbf{B}}(t') \gg^r = -i\theta(t-t') < [\hat{\mathbf{A}}(t), \hat{\mathbf{B}}(t')] > . \tag{2.2}$$

$$G_a(t,t') \equiv \ll \hat{\mathbf{A}}(t); \hat{\mathbf{B}}(t') \gg^a = +i\theta(t'-t) < [\hat{\mathbf{A}}(t), \hat{\mathbf{B}}(t')] > . \tag{2.3}$$

$$G_c(t,t') \equiv \ll \hat{\mathbf{A}}(t); \hat{\mathbf{B}}(t') \gg^c$$

$$= i\theta(t-t') < \hat{\mathbf{A}}(t), \hat{\mathbf{B}}(t') > +\eta i\theta(t'-t) < \hat{\mathbf{B}}(t'), \hat{\mathbf{A}}(t) > \tag{2.4}$$

Where$\ll ... \gg$ is the abbreviated notation for the Green functions, and$< ... >$ denotes averaging over a grand canonical ensemble. $\theta(t,t')$ is the step function.

$$\theta(t-t') = \begin{cases} 0, & t < t'; \\ 1, & t > t'. \end{cases} \tag{2.5}$$

Also **[A,B]** is a commutator or anti-commutator, that is, **[A,B]** = $AB - \eta BA$, $\eta = \pm 1$. The sign of η is positive if A and B are both **Bose** operator and negative if they are **Fermi** operators.

In our discussion we will use the Double-time Green function. In order to obtain the equation of motion we differentiate eq.(2.4) with respect to t as,

$$i\frac{d}{dt}G_r(t-t') = i\frac{d}{dt} \ll \hat{A}(t); \hat{B}(t') \gg$$
$$= \delta(t-t') < [\hat{A}(t); \hat{B}(t')] > + \ll [\hat{A}(t), \hat{H}]; \hat{B(t')} \gg . \tag{2.6}$$

Taking use of between Heaviside step function $\theta(t)$ and Dirac-δ function, $\theta(t) = \int_{-\infty}^{t} \delta(t)dt$, and $\frac{d}{dt}\theta(t) = \delta(t)$.

It is known that $A(t)$ and $B(t')$ satisfy equation of the form,

$$i\frac{dA}{dt} = [A, H].$$

Now equation of motion becomes,

$$i\frac{d}{dt}G_r(t-t') = \delta(t-t') < [\hat{A}(t); \hat{B}(t')] > + \ll \hat{A}(t)\hat{H} - \hat{H}\hat{A}(t); \hat{B}(t') \gg . \tag{2.7}$$

To solve this equation it is convenient to work with Fourier transform of this equation. A careful analysis shows that the function depends on t and t' through$(t-t')$. Thus we can write $G_r(t,t') = G_r(t-t')$.

Now let $G_r(\omega)$ be the Fourier transform of $G_r(t-t')$ such that

$$G_r(t-t') = \int_{-\infty}^{\infty} G_r(\omega) exp(-i\omega(t-t'))d\omega. \tag{2.8}$$

$$G_r(\omega) = \frac{1}{2\pi}\int_{-\infty}^{\infty} G_r(t-t') exp(i\omega(t-t')d(t-t'). \tag{2.9}$$

And the δ function can be defined as

$$\delta(t-t') = \frac{1}{2\pi}\int_{-\infty}^{\infty} exp(-i\omega(t-t')d\omega. \tag{2.10}$$

Equation(8) becomes,

$$\omega G(\omega) =< [A(t), B(t')] > + \ll [A(t), H]; B(t') \gg_{\omega} .$$

Since the fourier transform of G(t) is $G(t) = \int G(\omega)exp(-i\omega t)d\omega$ from which it can be shown that
$\frac{\partial G}{\partial t} = -i\omega$ [fourier transform of $G(t)$] Then $\omega G(\omega)$ can be written as

$$\omega \ll A, B \gg_{\omega} =< [A, B] > + \ll [A, H], B \gg_{\omega} . \tag{2.11}$$

Since $\ll A, B \gg_{\omega}$ denotes the Fourier transform of the Green functions involving the operator A and B. It satisfy the equation of motion eq.(2.6), where the double brackets $\ll ... \gg$ indicates the Fourier transform of the corresponding Green function. The single brackets $< ... >$ indicate the thermal average over the canonical ensemble, that is ,

$$< F >= \frac{Trexp(-\beta H)F}{Trexp(\beta H)}.$$

Where $\beta = 1/(k_B T)$, k_B is the boltzman constant. H is the hamiltonian of the system considered.
From the analytical properties of the Green functions it follows that the correlation function $< \hat{B}(t')A(t) >$ can be obtained from the equation of Green functions by

$$< \hat{B}(t')A(t) >= i \lim_{\epsilon \longrightarrow 0} \int_{-\infty}^{\infty} \frac{(\ll \hat{A}; \hat{B} \gg_{\hbar\omega+i\epsilon} - \ll \hat{A}; \hat{B} \gg_{\hbar\omega-i\epsilon})}{exp(\beta\hbar\omega) - 1}. \tag{2.12}$$

In order to obtain the superconductivity properties, we have defined super conducting order parameters, Δ (energy gap), which is pairing of electron or

spin and momentum by,

$$\Delta = \sum_k v < a_{k\uparrow} a_{-k\downarrow} > .$$

$$\Delta^* = \sum_k v < a^\dagger_{-k\downarrow} a^\dagger_{k\uparrow} > .$$

where $\Delta = \Delta^*$ (since Δ is real).

2.2 Experimental Method

2.2.1 Superconducting quantum interference device(SQUID)

Nowadays there are different measurement methods used to characterize and study the magnetic properties of superconducting materials. Among these there are devices which require motion of the sample, within or through a pickup coil (e.g., vibrating sample magnetometers VSM-SQUID), and those that measure a force or torque, in which case the sample is held stationary while the field is rotated or a gradient is applied (e.g.,torque magnetometers-SQUID magnetometry).

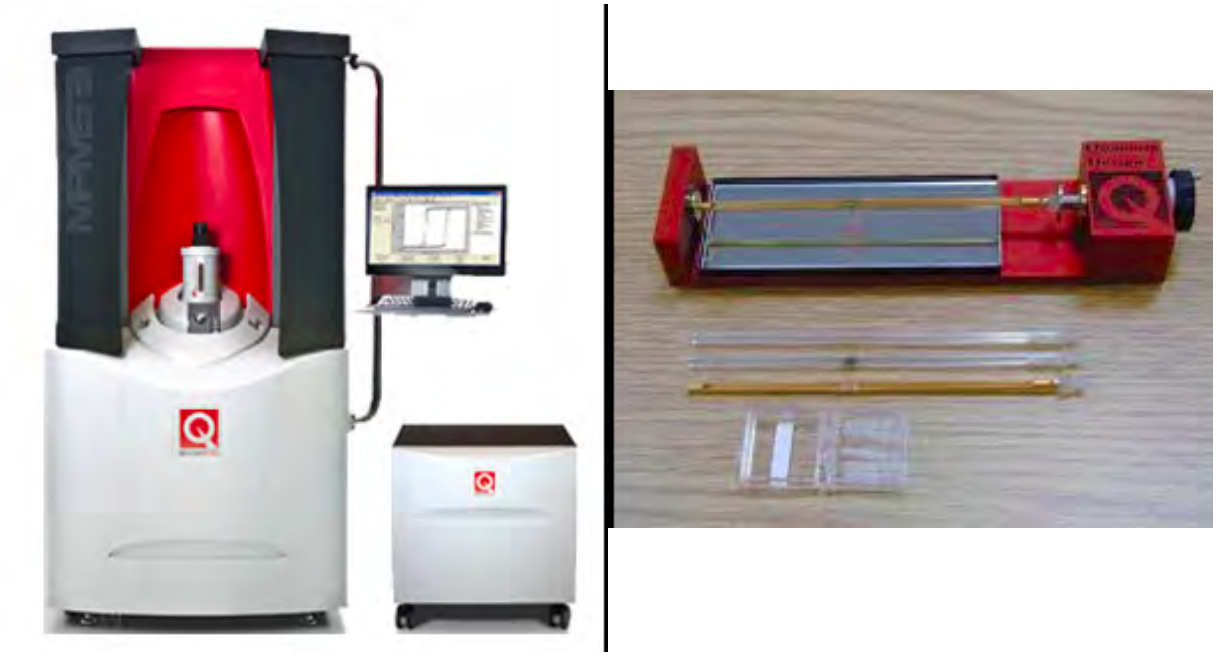

Figure 2.1: SQUID(left) and samples mounting(right)

Superconducting quantum interference device(SQUID) is one of the standard

technique in many laboratories. Parts of the result described in this thesis(chapter 4) were performed by VSM-SQUID. A SQUID (Fig 2.1a) is a very sensitive magnetometer used to measure small fields up to $5 \times 10^{-8}T$. A brief description of the instrument and working principle can be found from e.g., [14].

The SQUID VSM (vibrating sample magnetometer) is a device that measures magnetic properties, where a sample is placed inside a uniform magnetic field to magnetize it. Then it is physically vibrated sinusoidally. The induced voltage in the pickup coil is proportional to the sample's magnetic moment. According to Faraday's law, the change in the magnetic flux induces a voltage in the pickup coil:

$$V_{coil} = \frac{d\phi}{dt} \tag{2.13}$$

For a sinusoidally oscillating sample position, the voltage is based on the following equation:

$$V_{coil} = 2\pi f C m A sin(2\pi f t) \tag{2.14}$$

Where C is a coupling constant, m is the DC magnetic moment of the sample, A is the amplitude of oscillation, and f is the frequency of oscillation.

The Figure (Fig 2.2a) show the schematic diagram of the SQUID. The SQUID and magnet must both be cooled with liquid helium. Liquid helium is also used to cool the sample chamber, providing temperature control of samples from 400 down to 1.8 Kelvin. The SQUID VSM works with both cryogens liquid helium and liquid nitrogen.

2.2.2 Josephson junction

SQUID consists of Josephson junction in a superconducting ring. The discovery of Josephson effect opens a way for inventing SQUID. The Josephson junction is a junction between two superconductors which are weekly coupled separated by thin insulating barrier. Under this condition, cooper pairs of electrons can pass from one superconductor to the other even with no applied voltage. One of the principle associated with Josephson junctions is the quantization of the magnetic flux enclosed by a superconducting ring.

$$\Phi_0 = \frac{2\pi\hbar}{2e} \cong 2.0678 \times 10^{-15} T m^2 \tag{2.15}$$

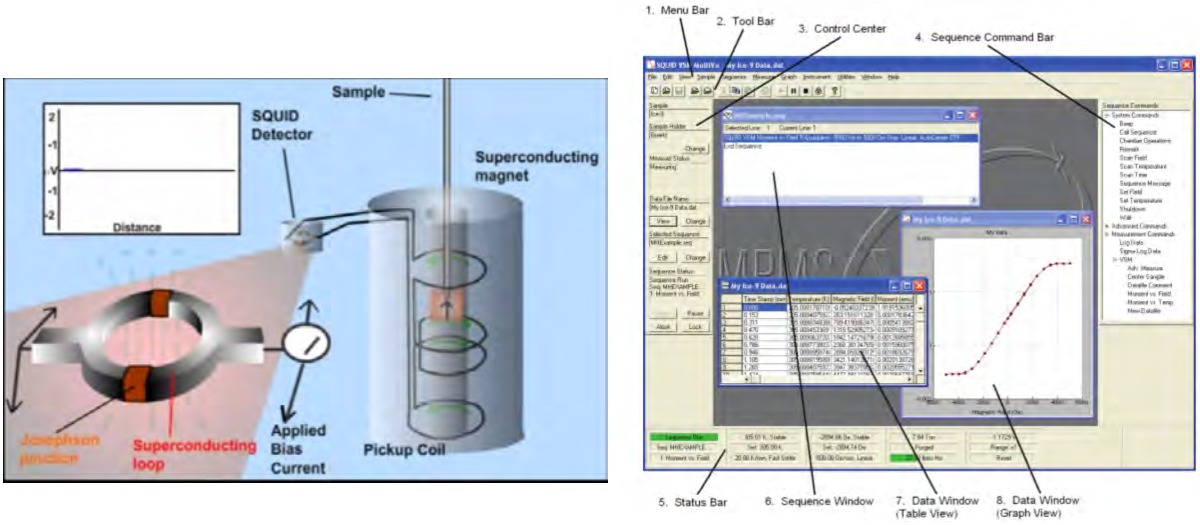

Figure 2.2: Schematic diagram of SQUID (left) and user interface overview (right)[14]

Basic steps

One of the first step to start measuring with the device is to refill it with liquid helium. The remaining most common tasks are Mounting sample(Fig 2.1b), Loading sample, Centering sample, and measuring sample. The computer then tell the progress of the measurement.

Software

MultiVu Windows software is the software that coordinates the operation of the SQUID VSM hardware. MultiVu combines in a single user interface the basic instrument control, status reporting, data collection, graphing, sequence editing and sequence execution. In addition to these features, MultiVu also contains instrument utilities, diagnostics, and error reporting. The main MultiVu window is shown in the figure(Fig. 2.2b).

The possible source of errors are loosely mounting sample, temperature error, and environmental source of errors.

2.2.3 Units

Here we present the most widely used units in experimental reports related to magnetism. The software of SQUID magnetometer outputs the magnetic

moment of a sample in electromagnetic units(emu).

$$1emu = 1Gcm^3 = 1erg/G \tag{2.16}$$

The unit conversion in the Gauss system, where the units of magnetic induction B and magnetic field H have the same magnitude,

$$1T = 10^4G = 10^4Oe \tag{2.17}$$

The molar magnetization M is expressed in units of

$$emu/mol = Gcm^3/mol, \tag{2.18}$$

and the molar magnetic susceptibility $\chi = M/H$, is expressed in units of

$$emu/(Oemol) = cm^3/mol. \tag{2.19}$$

2.3 First Principle Method - DFT

First principles method called Density Functional Theory (**DFT**) was introduced by Walter Kohn around 1965. For inventing this powerful technique he was awarded the Nobel prize in Chemistry in 1998. DFT is a commonly used method in condensed-matter physics, computational Physics, material science and quantum chemistry to describe properties of condensed matter systems. DFT is a useful method to understand and predict the properties of many materials. This method allows to study materials even with minimum input parameter like the atomic type and lattice parameters, and that is why it is also called first principle method.
A rapid success has been achieved in electronic structural calculation after DFT was introduced in 1960s. Here we give a short introduction.
In DFT, the assumption reduced the problem of studying a system of N electrons interacting with each other to the case of a system of N non-interacting electrons in an external potential. This was done by introducing the electronic density n(r) as the main variable instead of the full electronic wave function. The developent of DFT is based on the two theorems of Hohenberg and Kohn.

2.3.1 The Hohenberg-Kohn Theorems

First Hohenberg-Kohn theorem: *The ground state density n(r) of a many-body quantum system in some external potential v(r) uniquely determines the potential.*
Hence according to DFT, all properties of a many-body system can be determined by the ground state charge density.

$$\Psi\{r_1, ...r_n\} \rightarrow n(r) = \sum_i \mid \varphi_i(r) \mid^2 \tag{2.20}$$

Second Hohenberg-Kohn theorem: *The ground state energy E is also uniquely determined by the ground-state charge density: the density that minimizes the total energy is the exact ground state density.*

$$E[n(r)] =< \psi|T + U + V|\psi >=< \psi|T + U|\psi > + < \psi|V|\psi >$$

$$= F[n(r)] + \int n(r)v(r)dr \tag{2.21}$$

Where H = T + U + V , is the many-electron Hamiltonian, ψ is ground state wave function, T is the kinetic energy, U is the electron- electron interaction, V is the external potential, and n(r) is the charge density. The universal functional F of the density is $F[n(r)] =< \psi|T + U|\psi >$. The Functional includes the kinetic energy of the electrons $T_s[n]$, Hartree classical Coulomb repulsion energy $E_H[n]$, and the exchange and correlation energies $E_{xc}[n]$.

$$F[n(r)] = T_s[n] + E_H[n] + E_{xc}[n] \tag{2.22}$$

2.3.2 Kohn-Sham equation

In 1965, Kohn and Sham showed that it is possible to reduce the many-body quantum mechanical problem to an exactly equivalent set of one-electron equations, solved self- consistently. This is a reformulation of the following idea. The system of interacting electrons is mapped on to an auxiliary system of non-interacting electrons having the same ground state charge density n(r). In Kohn-Sham equation the Schrodingers equation for the system takes the

following form:

$$[-\frac{\hbar^2}{2m}\bigtriangledown^2 + V(r)_{ion} + V(r)_H + V_{XC}[n(r)]]\varphi_i(r) = \epsilon_i\varphi_i(r) \tag{2.23}$$

The first term is the energy of non-interacting electrons. The second term $V(r)_{ion}$ is the ionic potential describing the attractive interaction between electrons and nuclei. The third term (called the Hartree potential) contains the electrostatic interactions between clouds of charge.

$$V(r)_H = \int \frac{e^2 n(r')}{|r - r'|} d^3r' \tag{2.24}$$

The fourth term is called the exchange and correlation potential.

$$V_{XC}[n(r)] = \frac{\delta E_{xc}}{\delta n(r)} \tag{2.25}$$

The nature of this external potential defines the physical properties of the system and thus is extremely important. Ground state electronic energies ϵ_i and wave functions $\varphi_i = |i, k >$ can be obtained as the result of the DFT calculation.

In many cases very good agreement with experiment is achieved when the exchange and correlation potential is treated using the rather simple local density approximation (LDA) [20, 21]. A large variety of important scientific results have been and are still being obtained using LDA and the generalized gradient approximations (GGA).

2.3.3 Local Density Approximation(LDA)

Local Density Approximation is the simplest class of approximation in exchange - correlation functional. It is derived from homogeneous electron gas model. Generally, for a spin-unpolarized system, the local-density approximation for the xc energy is expressed as:

$$E_{xc}^{LDA}[n] = \int \varepsilon_{xc}^{hom}(n(r))n(r)dr \tag{2.26}$$

The exact exchange-correlation energy for the homogeneous electron gas was computed by Cperley and Alder using the Quantum Monte Carlo method,

which was then parameterized in a functional form by Perdew and Zunger.
The Local Density approximation can further be extended to an other approximation called Local Spin Density Approximation (LDA) for the treatments of magnetic materials. In this case the spin-dependence of the correlation energy density is computed by introducing the relative spin-polarization.
LDA is powerful in describing many properties of systems. But it has also a limitation based on the assumption that the electron density around an atom to be homogeneous.

Generalized Gradient Approximation(GGA)

This approach includes more physical information than LDA. It is expressed as

$$E_{xc}^{GGA}[n] = \int \varepsilon_{xc}^{GGA}(n(r), |\nabla n(r)|)n(r)dr \tag{2.27}$$

There are two commonly used functionals in calculations involving solids. These are the Perdew Wang functional (PW91) and the Perdew Burke Ernzerhof functional (PBE).
In summary, in order to better describe correlation effects in some strongly correlated systems such as compounds with transition metals (3d electrons) and lanthanide (4f electrons), several extensions to LDA and GGA have been made. Such as Coulomb parameter U and Hunds exchange parameter J are included for the d and f electrons, LDA+U, etc.

2.3.4 plane wave basis set and Pseudopotentials

A plane wave basis set is defined as

$$< r|k+G >= \frac{1}{\sqrt{V}} e^{i(k+G).r}, \tag{2.28}$$

$$\frac{\hbar^2}{2m}|k+G|^2 < E_{cut}, \tag{2.29}$$

where G is the reciprocal vector, V is the crystal volume, E_{cut} is a cutoff on the kinetic energy of PW's. PWs are simple to use and the basis is fixed by the crystal structure and by the cutoff. It allows to check the convergence by changing the cutoff.

The concept of Pseudopotentials have been widely applied in condensed matter Physics. The pseudopotential method is based on the fact that the valence electrons are responsible for most chemical and physical properties of molecules and solids. There are different Pseudopotentials, including norm-conserving and ultrasoft.

2.3.5 Self-consistent algorithm

Fig. 2.3 schematically illustrates the major steps of a density-functional self-consistent loop. It is known that Density Functional Theory is a self-consistent field (SCF) method. This means that the calculation runs in cycles, and convergence is achieved when the results given by solving the SCF equations are consistent with the assumptions made at the beginning of the cycle. In DFT the main quantity that is calculated and checked for self-consistency, is the electronic density.

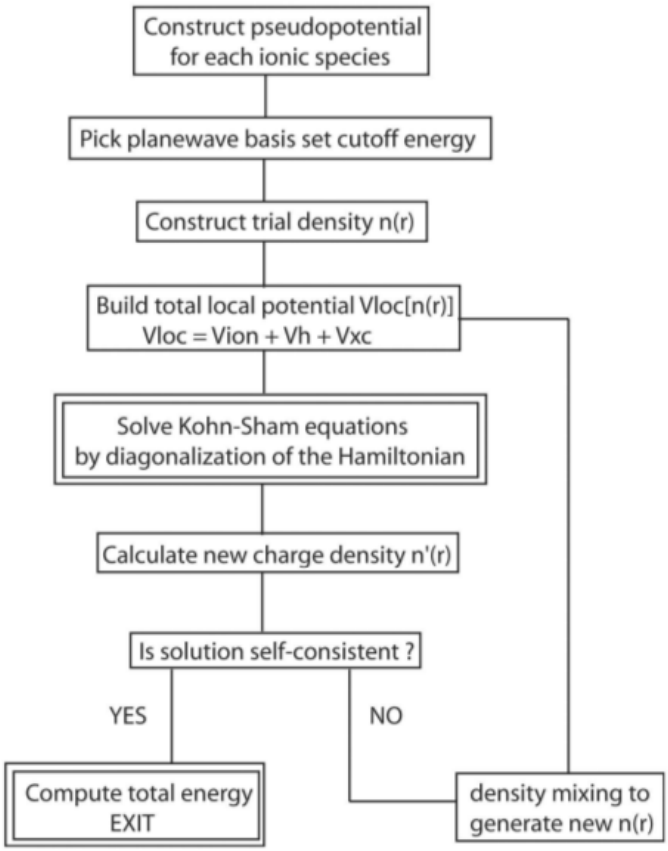

Figure 2.3: Schematic representation of the self-consistent algorithm for a density-functional based calculation

2.3.6 Brillouin zone

The Brillouin zone is important in plane-wave DFT calculations. The Brillouin zone plays an important role in electronic structure calculations. Several points in the Brillouin zone of band structures are given separate names. The most important of these is where **k** = 0; this location in k space is called the Γ point. The volume of the primitive cell in real space defined by the WignerSeitz construction,

$$V_{BZ} = \frac{(2\pi)^3}{V_{cell}}. \tag{2.30}$$

Chapter 3

Theoretical Study of the Interplay of Superconductivity and Magnetism in Fe Based Superconductors

ABSTRACT

The interplay of superconductivity and magnetism studied in iron based superconductor using the Hamiltonian consisting of the itinerant electrons, localized electrons, and s-d interaction. Using Greens function technique and equation of motion, we have obtained an expressions for superconducting order parameters ($\Delta(T)$, $\Delta(0)$) and critical temperature T_C , which reduce to BCS result in the absence of magnetic interactions. The result of the calculations shows that superconductivity can coexist with magnetism in iron based superconductor below the critical temperature. The equation also indicates magnetization suppresses T_C, in agreement to experimental report. The result also suggest the importance of the concept of localized and itinerant electron system in theoretical work.

3.1 Introduction

The discovery of high T_C iron based superconductor in 2008 [3] leads to multidirectional investigation both from experimental as well as theoretical point of views. The interrelation between Superconductivity and magnetism has been an interesting topic in Condensed matter Physics. According to reviews on iron based superconductors [27, 28], magnetic interactions are important for understanding the mechanism of superconductivity. Experimental observation and theoretical prediction show that knowing the interplay of superconductivity and magnetism may suggest the possible mechanism of superconductivity. Superconductivity has been found by applying either external pressure and chemical doping. The effect of doping and external pressure is different for different compounds. In most iron based superconductors both electron and hole doping on parent compounds causes superconductivity. It was observed that magnetism suppressed by doping before the appearance of superconductivity in systems like $PrFeAsO_{1-x}F_x$, and $CeFeAsO_{1-x}F_x$ [29, 30, 31, 29]. It was also reported that magnetism gradually disappears with a decrease in the spin density wave transition temperature [32] because of doping.

Generally substitution of element in most FeAs-based compounds may lead to suppression of spin density wave and eventual appearance of superconductivity [15, 33]. Fig(1.3, 1.4) indicates the phase diagram of Iron based

superconductors as a function of doping with structural and magnetic phase transitions.

Experimental reports show that superconductivity coexists with magnetism in a number of FePn/Ch superconductors including $SrFe_{2-x}Rh_xAs_2$ and others [34, 45, 46]. The Coexistence could occur with in the same electron system or different electron system based on the amount of dopant concentration.

In general the mechanism of high-Tc superconductivity has not been yet understood theoretically. There are a number of questions that should be answered in order to push Tc to room temperature. The phase diagrams show that upon doping or applying pressure the magnetic nature of the superconducting compound changes, but the nature of this transition still not understood well.

The other important question is that, since the coexistence on the phase diagrams for a number of Iron-based superconductor is seen(Fig 1.4), it is not completely understood whether magnetism and superconductivity evolve from the same itinerant/localized electrons or not.

There are different theoretical attempt to answer these and other questions.

Here using Green functions method we study the interplay of superconductivity and magnetism on iron based superconductors which can help in explaining experimental observations. In particular we derive an expression for Tc in terms of magnetic term.

The Hamiltonian of our model considers both itinerant and local electrons system. This is because many theories have been suggesting that the origin of the magnetism in iron-based superconductors could be both itinerant-electron and local-moment magnetism.

Magnetism from itinerant electrons was proposed by theories and experiments, because the cylinder-like electron-type pockets of the Fermi surface and hole-type ones are separated by a two-dimensional commensurate nesting vector, (π, π), in the Brillouin zone [35, 36, 37]. Where as magnetism from local moments is based on the Heisenberg-type interaction between localized spin moments [38, 39]. In this work we will follow a combined model.

3.2 The Model Hamiltonian and the calculation

(*This calculation was published on World Journal of Condensed Matter Physics, 4, 53-57(2014)*)
Our model Hamiltonian is

$$H = H_p + H_l + H_{el}. \tag{3.1}$$

Where the first term $H_p = \sum_{k,\sigma} \varepsilon(k)\hat{a}^{\dagger}_{k\sigma}\hat{a}_{k\sigma} - \Sigma_{kk'}V_{kk'}\hat{a}^{\dagger}_{k\uparrow}\hat{a}^{\dagger}_{-k\downarrow}\hat{a}_{-k'\downarrow}\hat{a}_{k'\uparrow}$. In the above pairing Hamiltonian the term $\sum_{k,\sigma} \varepsilon(k)\hat{a}^{\dagger}_{k\sigma}\hat{a}_{k\sigma}$ describes the Hamiltonian of total energy of the itinerant electrons in one electron band approximation [44]. Here the operator $\hat{a}^{\dagger}_{k\sigma}(\hat{a}_{k\sigma})$ creates (annihilates) an electron with the wave vector k and the spin projection on z-axis $\sigma =\uparrow$ or $\downarrow$; $V_{kk'}$ is the pairing potential.
The second term ($H_l = \Sigma_{i,j} JS_i \bullet S_j$) describes the predominant interaction between the local moment by Heisenberg like model, and we considered only the nearest neighbor interaction. Here J is the nearest neighbor exchange that bridge by the As ions and it could be anti ferromagnetic in nature.
The third term ($H_{el} = -g\sum_i \sigma_i \bullet S_i$) describes the interaction between the spin σ_i of the itinerant electrons and the five 3d spin S_i local moment located at site i, where g is the corresponding exchange constant.
To get an effective interaction we change the momentum term in to boson operator. Diagonalizing the Hamiltonian(H_l) using Bogoliubov transformation,

$$a_k = u_k b_k + v_k b^{\dagger}_{-k},$$

for boson,

$$|u_k|^2 - |v_k|^2 = 1.$$

This can be parametrized by hyperbolic angle $u_k = cosh\theta_k$, $v_k = sinh\theta_k$, which is real and even under $k \longrightarrow -k$. The canonical form of the Hamiltonian in terms of spin waves,

$$H_l = E_o + \sum_k \omega_k \hat{b}^{\dagger}_k \hat{b}_k. \tag{3.2}$$

We obtained the itinerant electrons and localized electrons moment using relations in spin operators like, $S_i^\sigma = a_{i\sigma}^\dagger a_{i-\sigma}$, $\frac{1}{\hbar}\sigma_i^\dagger = a_{i\downarrow}^\dagger a_{i\uparrow}$, $\frac{1}{\hbar}\sigma_i^z = \frac{1}{2}\sum_\sigma z_\sigma n_{i\sigma}; (z_\uparrow = +1; z_\downarrow = -1)$. The electrons in the valence band which are interacting with an anti ferromagnetically ordered, localized spin system can be described by

$$H_{el} = -\frac{1}{2} g < S^z > \sum_{k\sigma} \hat{a}_{k\sigma}^\dagger \hat{a}_{k\sigma}. \tag{3.3}$$

We get an effective Hamiltonian

$$H_{eff} = \sum_{k\sigma} \varepsilon(k) \hat{a}_{k\sigma}^\dagger \hat{a}_{k\sigma} - \Sigma_{kk'} V_{kk'} \hat{a}_{k\uparrow}^\dagger \hat{a}_{-k\downarrow}^\dagger \hat{a}_{-k'\downarrow} \hat{a}_{k'\uparrow} + E_0 + \Sigma_k \omega_k \hat{b}_k^\dagger \hat{b}_k - \frac{1}{2} g\hbar < S^z > \sum_{k\sigma} \hat{a}_{k\sigma}^\dagger \hat{a}_{k\sigma}. \tag{3.4}$$

In order to calculate the superconducting parameter equation (2.11),

$$\omega G(\omega) = \omega \ll A, B \gg_\omega = < [A, B] > + \ll [A, H], B \gg_\omega,$$

will be used. Applying the above relations, the equations of motion for $\ll \hat{a}_{-k\downarrow}^\dagger, \hat{a}_{k'\uparrow}^\dagger \gg$ is

$$\omega \ll \hat{a}_{-k\downarrow}^\dagger, \hat{a}_{k'\uparrow}^\dagger \gg = [\hat{a}_{-k\downarrow}^\dagger, \hat{a}_{k'\uparrow}^\dagger] + \ll [\hat{a}_{-k\downarrow}^\dagger \hat{H}_{eff}]; \hat{a}_{k'\uparrow}^\dagger \gg . \tag{3.5}$$

This equation can be reduced with the use of the following properties,

$$[a_k, a_{k'}^\dagger] = \delta_{kk'} = 1, if, k = k', otherwise = 0.$$

$$[a_k, a_k] = [a_k^\dagger, a_k^\dagger] = 0.$$

The first term in the RHS goes zero but we still need to simplify $[\hat{a}_{-k\downarrow}^\dagger, \hat{H}_{eff}]$. To this end we need to apply elementary commutation relations.
Starting from the first term of H_{eff},

$$[\hat{a}_{-k\downarrow}^\dagger, -\sum_{k\sigma} \varepsilon(k) \hat{a}_{k\sigma}^\dagger \hat{a}_{k\sigma}] = -\sum_k \varepsilon(k) \hat{a}_{k\sigma}^\dagger \{\hat{a}_{-k\downarrow}^\dagger \hat{a}_{k\sigma}\} + \sum_k \varepsilon(k) \{\hat{a}_{-k\downarrow}^\dagger \hat{a}_{k\sigma}^\dagger\} a_{k\sigma}$$

$$= -\sum_{k} \varepsilon(k) \hat{a}^{\dagger}_{k\sigma} \sigma_{-kk} \sigma_{\downarrow\sigma} = -\varepsilon_{-k} \hat{a}^{\dagger}_{-k\downarrow}, \tag{3.6}$$

for the case where -k = k and $\sigma = \downarrow$.

Similarly applying elementary commutation relations, the second term of H_{eff},

$$[\hat{a}^{\dagger}_{-k\downarrow}, -\sum_{kk'} V_{kk'} \hat{a}^{\dagger}_{k\uparrow} \hat{a}^{\dagger}_{-k\downarrow} \hat{a}_{-k'\downarrow} \hat{a}_{k'\uparrow}] = -\sum_{kk'} V_{kk'} \hat{a}^{\dagger}_{k\uparrow} \hat{a}^{\dagger}_{-k\downarrow} [\hat{a}^{\dagger}_{-k\downarrow}, \hat{a}_{-k'\downarrow} \hat{a}_{k'\uparrow}]$$

$$= -\sum_{kk'} V_{kk'} \hat{a}^{\dagger}_{k\uparrow} \hat{a}^{\dagger}_{-k\downarrow} (\{\hat{a}^{\dagger}_{-k\downarrow} \hat{a}_{-k'\downarrow}\} \hat{a}_{k'\uparrow} - \hat{a}^{\dagger}_{-k\downarrow} \{\hat{a}_{-k'\downarrow} \hat{a}_{k'\uparrow}\})$$

$$= -\sum V_{kk'} \hat{a}^{\dagger}_{k\uparrow} \hat{a}^{\dagger}_{-k\downarrow} a_{k'\uparrow}. \tag{3.7}$$

Similarly for the third term of H_{eff},

$$[\hat{a}^{\dagger}_{-k\downarrow}, (E_o + \Sigma_k \omega_k \hat{b}^{\dagger}_k \hat{b}_k)] = 0, \tag{3.8}$$

and finally the fourth term becomes,

$$[\hat{a}^{\dagger}_{-k\downarrow}, -\frac{1}{2} g\hbar < S^z > \sum_{k\sigma} \hat{a}^{\dagger}_{k\sigma} \hat{a}_{k\sigma}]$$

$$= \frac{1}{2} g\hbar < S^z > \hat{a}^{\dagger}_{-k\downarrow}. \tag{3.9}$$

With these results,

$$[\hat{a}^{\dagger}_{-k\downarrow}, \hat{H_{eff}}] = (\frac{1}{2} g\hbar < S^z > -\varepsilon_{-k}) \hat{a}^{\dagger}_{-k\downarrow} - \sum V_{kk'} \hat{a}^{\dagger}_{k\uparrow} \hat{a}^{\dagger}_{-k\downarrow} a_{k'\uparrow}. \tag{3.10}$$

Hence, equation (3.5) becomes,

$$\omega \ll \hat{a}^{\dagger}_{-k\downarrow}, \hat{a}^{\dagger}_{k'\uparrow} \gg = (-\varepsilon_{-k} + \frac{1}{2} g\hbar < S^z >) \ll \hat{a}^{\dagger}_{-k\downarrow} \hat{a}^{\dagger}_{k'\uparrow} \gg - \sum V_{kk'} \ll \hat{a}^{\dagger}_{k\uparrow} \hat{a}^{\dagger}_{-k\downarrow} a_{k'\uparrow} \hat{a}^{\dagger}_{k'\uparrow} \gg .$$

Applying decoupling for the last term in the above equation gives,

$$(\omega + \varepsilon_{-k} - \frac{1}{2} g\hbar < S^z >) \ll \hat{a}^{\dagger}_{-k\downarrow}, \hat{a}^{\dagger}_{k'\uparrow} \gg = -\sum V_{kk'} < \hat{a}^{\dagger}_{k\uparrow} \hat{a}^{\dagger}_{-k\downarrow} > \ll a_{k'\uparrow} \hat{a}^{\dagger}_{k'\uparrow} \gg$$

$$= -\Delta^* \ll a_{k'\uparrow} \hat{a}^{\dagger}_{k'\uparrow} \gg . \tag{3.11}$$

Applying the same techniques and procedure we need to find an expression for $\ll \hat{a}_{k'\uparrow}, \hat{a}^{\dagger}_{k'\uparrow} \gg$. Using H_{eff},

$$\ll \hat{a}_{k'\uparrow}, \hat{a}^{\dagger}_{k'\uparrow} \gg = 1 + \ll [\hat{a}_{k'\uparrow}, \hat{H}_{eff}], \hat{a}^{\dagger}_{k'\uparrow} \gg . \tag{3.12}$$

To simplify this we need to do first $[\hat{a}_{k'\uparrow}, \hat{H}_{eff}]$

$$[\hat{a}_{k'\uparrow}, \hat{H}_{eff}] = \varepsilon_k a_{k'\uparrow} - \frac{1}{2} g\hbar < S^z > a_{k'\uparrow} - V_{kk'} \hat{a}^{\dagger}_{-k\downarrow} \hat{a}_{k'\downarrow} \hat{a}_{k'\uparrow}$$

Hence,

$$\omega \ll \hat{a}_{k'\uparrow}, \hat{a}^{\dagger}_{k'\uparrow} \gg = 1 + (\varepsilon_k - \frac{1}{2} g\hbar < S^z >) \ll \hat{a}_{k'\uparrow}, \hat{a}^{\dagger}_{k'\uparrow} \gg$$
$$-V_{kk'} \ll \hat{a}^{\dagger}_{-k\downarrow} \hat{a}_{k'\downarrow} \hat{a}_{k'\uparrow}, \hat{a}^{\dagger}_{k'\uparrow} \gg .$$

After applying cycling and decoupling on the last term, the above equation can be rewritten as

$$(\omega - \varepsilon_k + \frac{1}{2} g\hbar < S^z >) \ll \hat{a}_{k'\uparrow}, \hat{a}^{\dagger}_{k'\uparrow} \gg = 1 - V_{kk'} < \hat{a}_{-k'\downarrow} \hat{a}_{k'\uparrow} > \ll \hat{a}^{\dagger}_{-k\downarrow} \hat{a}^{\dagger}_{k'\uparrow} \gg$$

$$= 1 - \Delta \ll \hat{a}^{\dagger}_{-k\downarrow} \hat{a}^{\dagger}_{k'\uparrow} \gg . \tag{3.13}$$

In general from equation (3.11) and (3.13) we found the following two equations (for $\Delta = \Delta^*$ and $\varepsilon_{-k} = \varepsilon_k$).

$$(\omega - \varepsilon) \ll \hat{a}^{\dagger}_{-k\downarrow}, \hat{a}^{\dagger}_{k'\uparrow} \gg = -\Delta \ll \hat{a}_{k'\uparrow}, \hat{a}^{\dagger}_{k'\uparrow} \gg \tag{3.14}$$

$$(\omega + \varepsilon) \ll \hat{a}_{k'\uparrow}, \hat{a}^{\dagger}_{k'\uparrow} \gg = 1 - \Delta \ll \hat{a}^{\dagger}_{-k\downarrow}, \hat{a}^{\dagger}_{k'\uparrow} \gg . \tag{3.15}$$

From these we get

$$<< \hat{a}^{\dagger}_{-k\downarrow}, \hat{a}^{\dagger}_{k'\uparrow} >> = \frac{-\Delta}{\omega^2 - \varepsilon^2 - \Delta^2}. \tag{3.16}$$

Where $\varepsilon = \varepsilon_k - \frac{1}{2} g\hbar < S^z >$.
The superconducting order parameter is defined as

$$\Delta = \Sigma_{k,n} \frac{V_{kk'}}{\beta} \ll \hat{a}^{\dagger}_{-k\downarrow}, \hat{a}^{\dagger}_{k'\uparrow} \gg . \tag{3.17}$$

The sum may be changed to integral by introducing the density of state

$N(\epsilon)$, and equation (3.17) becomes

$$1 = \frac{1}{\beta}\sum\int d\varepsilon_0 N(\varepsilon) V_{kk'}[\frac{-1}{\omega^2 - \varepsilon^2 - \Delta^2}]. \tag{3.18}$$

Attractive interaction is effective for the region $-\hbar\omega_0 < \varepsilon < \hbar\omega_0$, and assuming the density of states does not vary over this integral, the expression becomes,

$$\frac{1}{\lambda} = \int_0^{\hbar\omega_0} \frac{2}{\beta}\sum_0^{\infty} \frac{-1}{\omega^2 - \varepsilon^2 - \Delta^2}. \tag{3.19}$$

Applying Laplaces transform with replacement of ω by Matsubara frequency $\omega_n = (2n+1)\pi/\beta$, and using the approximation,

$\frac{1}{\omega_n^2+\varepsilon^2+\Delta^2} \simeq \frac{1}{\omega_n^2+\varepsilon^2} - \frac{\Delta^2}{(\omega_n^2+\varepsilon^2)^2}$.

The equation becomes

$$\frac{1}{\lambda} = \int_0^{\hbar\omega_0} d\varepsilon \frac{tanh(\beta/2)\varepsilon}{\varepsilon} - 4\Delta^2 \sum_{n=0}^{\infty} (\frac{\beta}{\pi(2n+1)^2})^3 \int_0^{\infty} \frac{1}{(1+x^2)^2} dx. \tag{3.20}$$

where $x = \varepsilon/a, a = (2n+1)\pi/\beta$.

For low temperature the first integral becomes

$$I_1 = ln\frac{1.13}{K_B T}(\hbar\omega_0 - \tfrac{1}{2}g\hbar < S^z >).$$

The second integral becomes

$$I_2 = 1.05(\tfrac{\Delta}{\pi K_B T})^2.$$

Hence

$$\frac{1}{\lambda} = ln\frac{1.13}{K_B T}(\hbar\omega_0 - \frac{1}{2}g\hbar < S^z >) - 1.05(\frac{\Delta}{\pi K_B T})^2.$$

This expression can be rewritten as

$$K_B T = 1.13(\hbar\omega_0 - \frac{1}{2}g\hbar < S^z >) e^{-[\frac{1}{\lambda} + (\frac{\Delta}{\pi K_B T})^2]}. \tag{3.21}$$

3.3 Result and Discussion

From this equation we can get the following important relations.
(i) Superconducting order parameter as a function of temperature

$$\Delta(T) = \pi K_B T \sqrt{(ln \frac{1.13(\hbar\omega_0 - \frac{1}{2}g\hbar < S^z >)}{K_B T}) - \frac{1}{\lambda}}. \tag{3.22}$$

This quantity (Δ) is zero at critical temperature T_C. Substituting $\Delta = 0$, we get

$$K_B T_C = 1.13(\hbar\omega_0 - \frac{1}{2}g\hbar < S^z >)e^{-1/\lambda}. \tag{3.23}$$

(ii) Using $ln(1-x) = -x - x^2/2 + ...$, $lnT/T_C \approx -(1 - T/T_C)$ we get the well known equation

$$\Delta(T) = 3.06 K_B T_C (1 - \frac{T}{T_C})^2$$

or

$$ln(T_C/T) = \frac{\Delta^2}{\pi^2 K_B^2 T^2}. \tag{3.24}$$

(iii) Equation (31) can be written as

$$\frac{1}{\lambda} = \int_0^{\hbar\omega_0} d\varepsilon \frac{tanh\beta/2\sqrt{\varepsilon^2 + \Delta^2}}{\sqrt{\varepsilon^2 + \Delta^2}}. \tag{3.25}$$

As $T \to 0$, $\beta \to \infty$, gives

$$\frac{1}{\lambda} = \int \frac{d\varepsilon}{\sqrt{\varepsilon^2 + \Delta^2}}. \tag{3.26}$$

Applying standard integrals and approximation for $x << 1$, and $(1+x)^n \approx 1+nx$, we get

$$\Delta(T \to 0) = \sqrt{4(\hbar\omega_0)^2 exp(-1/\lambda) - (\frac{1}{2}g\hbar < S^z >)^2}. \tag{3.27}$$

3.4 Conclusion

Equation (3.23) is clearly in agreement with the fact that as the net magnetization increases, superconductivity decreases. In addition to this, in the absence of magnetic term equations (3.23) reduces to the well known BCS expression.

The result clearly indicate that superconductivity can coexist with magnetism in iron based superconductor below the critical temperature. Experimental findings show the coexistence of superconductivity and magnetism in some range of doping in some compounds [34, 45, 46]. Our theoretical predictions are in broad agreement with experimental findings [34, 45, 46] and the result may help in explaining experimental observations.

Chapter 4

The effect of Y and Mn doping in La1111 superconductors

ABSTRACT

In this work we focus to study on the effect of Manganese(Mn) and Yttrium(Y) doping on Fe and La site respectively, for $La_{1-x}Y_xFe_{1-y}Mn_yAsO_{0.89}F_{0.11}$ series of samples. The magnetization measurement were done by using 7T VSM-SQUID. We took the data at 10Oe from 1.8k to 40k in ZFC and FC condition, and from 1.8 to 300k at 1T. We determined the T_C of different samples.

We specifically report the effect of Mn and Y simultaneous doping on the magnetic properties and superconducting critical temperature of the La series. Our results indicate that Y doping has a stabilizing effect on Superconductivity even in the presence of Mn doping. Mn has a pair breaking effect than Y because we found that a small amount of Mn suppresses Superconductivity very quickly. The superconducting critical temperature can not be expressed only in terms of amount of impurities but also in terms of the magnetic behavior of the dopant atom.

4.1 Introduction

The onset of superconductivity in different families of iron based compound arose an interest to understand the pairing mechanism in order to push T_C to room temperature. But until now there is no clear understanding of the superconducting pairing mechanism. In the previous chapter we tried to obtain an expression for T_C in terms of magnetic term with various approximations. The result motivated us to further study IBS systems by magnetization measurements.

In fact different approaches have been applied to understand the mechanism and to increase superconducting transition temperature(T_C). Typical example that shows the induction of superconductivity are (i) electron doping on LnFeAsO (Ln = La, Dy, Tb, Gd, Sm, Nd, Pr, Ce), with partial substitution of O by F; (ii) hole doping on $La_{1-x}Sr_xFeAsO$ (T_C = 25K) [47] and in $Nd_{1-x}Sr_xFeAsO$ (T_C = 13.5K) [48]; (iii) and by applying pressure for example, applying 4GP in $LaAsFeO_{0.89}F_{0.11}$(T_C = 43K) [49]. Oxygen deficiency in La1111 under pressure also shows an increase in Tc [50]. From different attempt the highest critical temperature (T_C = 56K) was announced in electron doping for instance in $Gd_{0.8}Th_{0.2}FeAsO$ compound [51], and $Ca_{0.4}Nd_{0.6}FeAsF$ [52]. On the other hand

the suppression of Tc by hole doping was reported upon substitution of Mn on Fe site [53].

The suppression effect of Mn atoms at low temperature gets attention due to its poisoning effect even at small amount of doping (x = 0.2%) [25]. The pair breaking effect due to the impurity atom is not well understood but the result of NMR and resistivity measurement indicates no charge doping rather localized magnetic impurities [54, 55].

The action of chemical pressure that distort lattice structure due to partial substitution of Yttrium(Y) in the Lanthanum (La) site of La1111 superconductor induce sc and surprisingly highest T_C recorded for a higher Y content. For example, 20% Y doped in $La_{0.8}Y_{0.2}FeAsO_{0.8}$ (T_C = 34K), and 40%Y doped $La_{0.8}Y_{0.2}FeAsO_{0.8}$ (T_C = 43K) [56]. The existed experimental result on lattice parameter would not explain the formation of cooper pair or the pairing symmetry due to the replacement of small atomic radii(Y). However it was reported that the increment of T_C is related to the change of a-axis and c-axis parameter [57], and when the As-Fe-As angle of FeAs tetrahedral approaches 109.47° [58]. This result demands optimizing Fermi surface topology.

So far there is no report on the computation of Y and Mn impurities when both doped on same compounds. That means the increment of T_C via lattice shrinkage in the presence of Y impurities and the poisoning effect of Mn atoms was not reported on same sample. We study where both Y and Mn are substituted on the same sample.

It was reported that there is a strong charge localization and Quantum critical point in La based system [25, 26]. Understanding the effect of chemical pressure through partial substitution of Y on La site and Mn on Fe site may suggest the possible reasons of pairing symmetry. The result of magnetization measurement may give a clue for the pair breaking effect of the impurity atoms.

In this paper we report on Mn and Y doped La1111 polycrystalline sample from data obtained by magnetization measurement using VSM-SQUID. In particular we focused on a series of $La_{1-x}Y_xFe_{1-y}Mn_yAsO_{0.89}F_{0.11}$ samples.

4.2 Experiments: VSM-SQUID

We did the measurement on polycrystalline sample grown in IFW Dresden, Germany. The Magnetization measurements were performed on polycrystalline sample using superconducting quantum interference device magnetometer (7T VSM-SQUID) from Quantum Design. A SQUID (superconducting quantum interference device) magnetometer is one of the most sensitive experimental techniques to magnetically characterize samples. It is used to measure small fields up to 5×10^{-8} T.

4.2.1 Experimental procedure

Sample preparation:

Polycrystalline samples $La_{1-x}Y_xFe_{1-y}Mn_yAsO_{1-z}F_z$ were prepared from mixtures of LaAs, YAs, Fe_2O_3, FeF_3, Fe and Mn at nominal molar ratios as described in detail in Ref. [59]. All the ingredients were milled, mixed and pressed into pellets under Ar atmosphere. The samples were heated in an evacuated silica tube at $940°C$ for 8 h and at $1150°C$ for 48 h. The annealed pellets were grind and polished and characterized with wavelength-dispersive X-ray spectroscopy (WDX).

Before any measurement we made a chemical analysis with Energy Dispersive X-ray spectroscopy(EDX). The general principle is analyzing the response while an incident radiation hits the sample. This techniques tells the composition of the sample to know the range of doping. We compare the nominal value with the estimated value obtained by EDX analysis.

Measurment:

We perform magnetization measurement on polycrystalline sample that were prepared based on the aforementioned techniques. We used the superconducting quantum interference device magnetometer (VSM-SQUID) from Quantum Design.

With this instrument one can have two basic measurements; (1) magnetization as a function of applied magnetic field, and (2) magnetization as a function of temperature. We took data in the temperature range 1.8-40K applying 10Oe in zero-field-cooled (ZFC) and in field-cooled (FC) conditions. We also obtained data for magnetization measurement in the temperature range from 1.8k to

300K in a magnetic field of 1T. The SQUID gives the magnetic moment of a sample in electromagnetic units (emu).
Before measuring the superconducting samples at low fields, the remnant field has been removed by applying 1 T and removing it by oscillatory mode.
The superconducting critical temperature was determined from zfc/fc susceptibility measurement. Its value was decided using the data of the diamagnetic susceptibility.

4.3 Result and Discussion

4.3.1 Magnetization measurement

Figure 4.1 and Fig 4.2 shows the diamagnetic volume susceptibility $4\pi\chi_V$ as a function of temperature for 20% Yttrium(Y) and 30%Y doping with different Manganese(Mn) (0, 0.1, 0.2, 0.3, 0.5, 0.8)% contents respectively. This value indicates the superconducting volume fraction of the samples we measured. Its value decreases with increasing the doping level for 30%Y, and similar for 20%Y except for 0.5% Mn. However the temperature dependence of all sample is very similar.
We compare the broadening of $4\pi\chi_V$ with the parent compound. It shows an increment at higher Mn content.
We tried to determine the superconducting width of 20%Y and 30%Y. The data of figure 4.1 and 4.2 indicates the superconducting transition widthΔT_C is a bit higher in 20%Y and increasing with Mn compared to 30%Y. The impact of impurities on superconducting nature can be expressed in terms of superconducting volume fraction.
From Fig.4.1 one can see that the superconducting volume fraction increases with increasing the Mn content up to 0.3 but decrease for 0.5 and then increase. There may be something wrong with sample quality of 0.50. But as shown in Fig. 4.2, the superconducting volume fraction increases with increasing Mn with respect to the absolute value -1. These indicates the poisoning effect of Mn even in the presence of Y which favors Superconductivity.

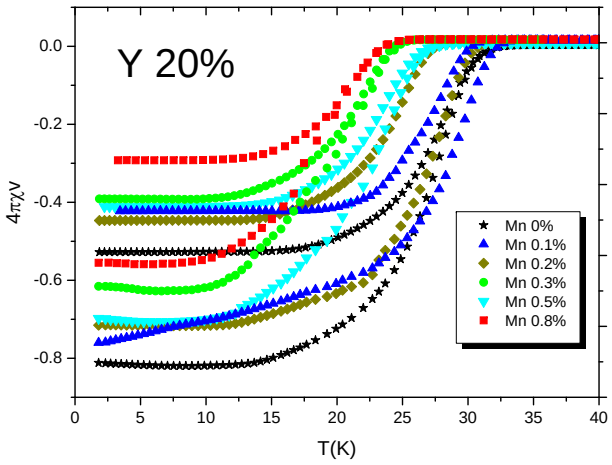

Figure 4.1: Volume susceptibility of polycrystalline sample of $La_{1-x}Y_xFe_{1-y}Mn_yAsO_{0.89}F_{0.11}$ series for 20%Y

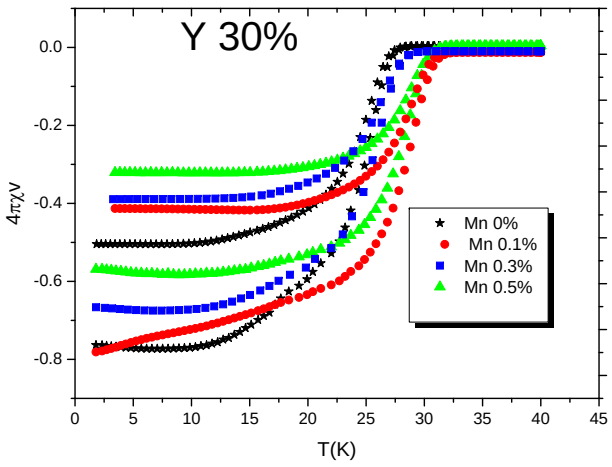

Figure 4.2: Volume susceptibility of polycrystalline sample of $La_{1-x}Y_xFe_{1-y}Mn_yAsO_{0.89}F_{0.11}$ series for 30%Y

4.3.2 Critical Temperature(T_C)

The superconducting critical temperature(T_C) was determined from zfc/fc susceptibility measurement. Its value was decided using the data of the diamagnetic susceptibility. The following figure(Fig. 4.3) shows how to determine T_C from the intercept of the solid line. This Magnetization curve versus temperature also displays the diamagnetic response (Meisner effect) below T_C. The

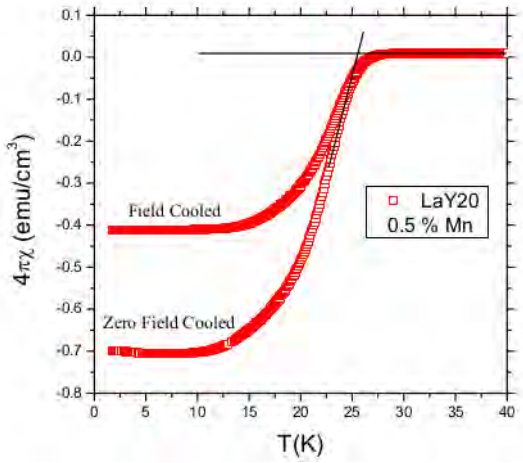

Figure 4.3: Typical example how to determine T_C from susceptibility per unit volume per temperature graph of $La_{0.8}Y_{0.2}Fe_{0.995}Mn_{0.005}AsO_{0.89}F_{0.11}$ sample

following table (table 4.1) shows the list of samples characterized by SQUID and EDX and the corresponding critical temperature.

The figure (4.4) shows Tc versus Manganese(Mn) content for 20% Yttrium(Y) doping samples with different Mn content (x= 0, 0.1, 0.2, 0.3, 0.5, 0.8)%. One can clearly see the quick suppression of Tc with small variation of Mn content. This may be the Mn strong pair breaking effect due to the localized ions. But the mechanism for this disappearance of Tc due to Mn atom is not clearly understood whether it is due to localized electrons or removal of Fermi surface or other.

For comparison purpose we measure with only Y doped and only with Mn doped samples. In the absence of Mn, Y doping induces superconductivity, for example, for 30% Y, Tc = 33k. But in the absence of Y, Mn doping suppress superconductivity, for example, for 0.5% Mn Tc = 10k and for 1% Mn superconductivity completely suppressed.

In Fig. (4.5) we present the effect of 0.5% Mn on a sample containing various amount of Y. The plot indicate that there is an increase in Tc with increasing

Table 4.1: Superconducting temperature Tc of different samples

Y 0.2 amount of doping	chemical formula	Tc
Mn=0	$La_{0.8}Y_{0.2}FeMn_0AsO_{0.89}F_{0.11}$	30.4
Mn=0.001	$La_{0.8}Y_{0.2}Fe_{0.999}Mn_{0.001}AsO_{0.89}F_{0.11}$	30.2k
Mn=0.002	$La_{0.8}Y_{0.2}Fe_{0.998}Mn_{0.002}AsO_{0.89}F_{0.11}$	30.2k
Mn=0.003	$La_{0.8}Y_{0.2}Fe_{0.997}Mn_{0.003}AsO_{0.89}F_{0.11}$	29.5k
Mn=0.005	$La_{0.8}Y_{0.2}Fe_{0.995}Mn_{0.005}AsO_{0.89}F_{0.11}$	25.5k
Mn=0.008	$La_{0.8}Y_{0.2}Fe_{0.992}Mn_{0.008}AsO_{0.89}F_{0.11}$	22k
Mn=0.015	$La_{0.8}Y_{0.2}Fe_{0.985}Mn_{0.015}AsO_{0.89}F_{0.11}$	20k
** Mn=0.02	$La_{0.8}Y_{0.2}Fe_{0.98}Mn_{0.02}AsO_{0.89}F_{0.11}$	15.7k
Y 0.3 amount of doping		
Mn=0	$La_{0.7}Y_{0.3}FeMn_0AsO_{0.89}F_{0.11}$	33k
Mn=0.001	$La_{0.7}Y_{0.3}Fe_{0.999}Mn_{0.001}AsO_{0.89}F_{0.11}$	29.5k
Mn=0.002	$La_{0.7}Y_{0.3}Fe_{0.998}Mn_{0.002}AsO_{0.89}F_{0.11}$	30.8k
Mn=0.003	$La_{0.7}Y_{0.3}Fe_{0.997}Mn_{0.003}AsO_{0.89}F_{0.11}$	26.2k
Mn=0.005	$La_{0.7}Y_{0.3}Fe_{0.995}Mn_{0.005}AsO_{0.89}F_{0.11}$	28.5k
Y 0 amount of doping		
Mn=0.005	$LaY_0Fe_{0.995}Mn_{0.005}AsO_{0.89}F_{0.11}$	10k
Mn=0.01	$LaY_0Fe_{0.99}Mn_{0.01}AsO_{0.89}F_{0.11}$	Not SC
Mn=0.02	$LaY_0Fe_{0.98}Mn_{0.02}AsO_{0.89}F_{0.11}$	Not SC
Y 0.0025, Mn=0.005	$La_{0.9975}Y_{0.0025}Fe_{0.995}Mn_{0.005}AsO_{0.89}F_{0.11}$	7.8k

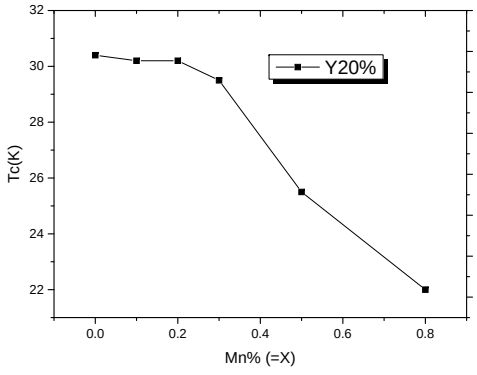

Figure 4.4: Tc versus Mn content of sample $La_{1-x}Y_xFe_{1-y}Mn_yAsO_{0.89}F_{0.11}$ series for 20%Y

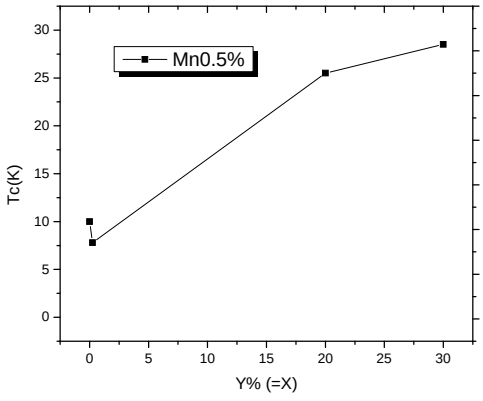

Figure 4.5: Tc versus Y content of sample $La_{1-x}Y_xFe_{0.5}Mn_{0.5}AsO_{0.89}F_{0.11}$ for 0.5Mn content

Y. The result shows that Yttrium(Y) doping stabilizes superconductivity even in the presence of small amounts of manganese(Mn).

It is observed that the chemical pressure has effect on the lattice parameters. Figure (4.6) shows the change of lattice parameter c with increasing the impurities Mn. This quick reduction in c-axis due to Mn doping result in suppressing Tc.

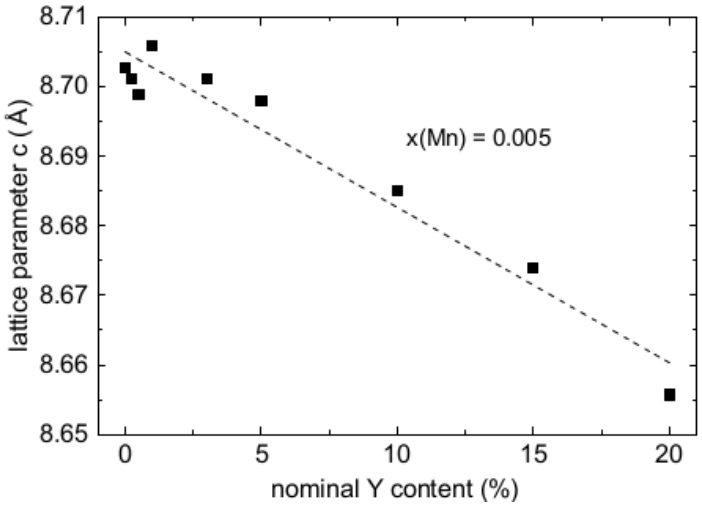

Figure 4.6: Change of lattice parameter c with increasing amount of Y for 0.5% of Mn

COMMENTS: 1. Magnetic transition

For different range of doping we observed the structural and/or magnetic phase transition around 120K (Fig. 4.8). This anomalies property of all sample can be easily seen by differentiating susceptibility with respect to temperature (fig 4.8). It is observed that the magnetic susceptibility linearly increases beyond the transition temperature, Tc in all samples and the data drops due to the onset of superconductivity at low temperature. It is difficult to say that this is because of the sample quality, since in all measured samples M vs H plot shows a uniformity(Fig 4.7). We observed a similar properties at 0.1T and 1T(Fig 4.8). This suggests that magnetic properties of La 1111 compound at 120K needs further examinations and better explanations.

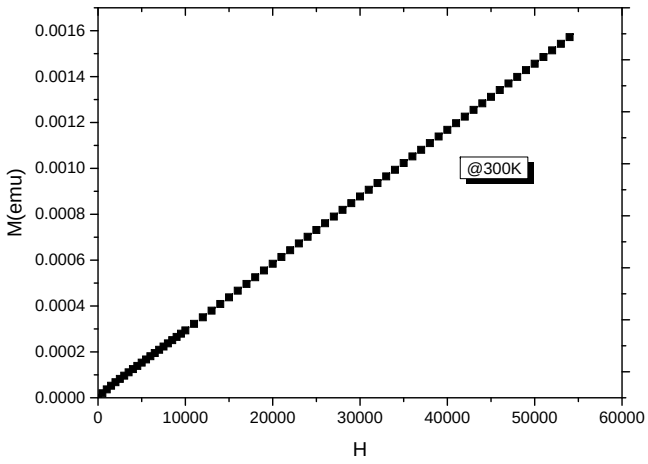

Figure 4.7: M versus H

COMMENTS: 2. Demagnetization correction

When measuring a superconducting sample it is often important to consider demagnetization effect.

The size and shape of the sample is important to precisely describe the magnetic response of a measured sample. The quantity that is determined from the shape of the sample is named as demagnetization factor. One can see the detail description how to find the demagnetization factor from the shape of the sample from reference [60]. Since the magnetization through the sample is not uniform, the internal magnetic field in a sample can be expressed as

$$H_{int} = H_{ext} - N_d M$$

Where N_d is the demagnetization factor. For sphere and ellipsoids it is possible to calculate, for others one needs to approximate. Our sample has neither of these shapes so we make an approximation.

We measured the dimensions of all samples by a computerized camera. See the typical photo in figure (4.9). We find by incorporating the assumption

$$a \geq b \geq c \geq 0$$

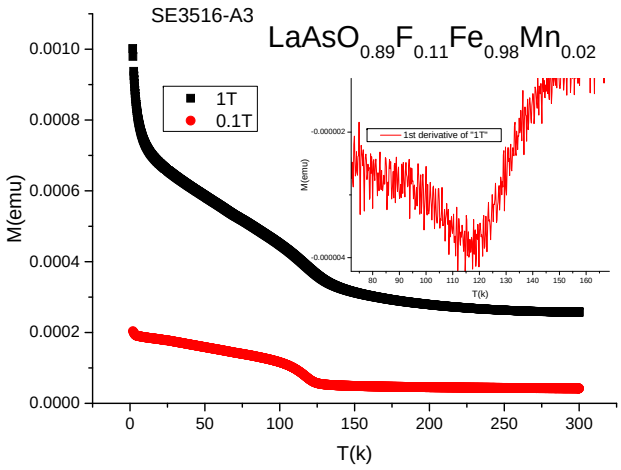

Figure 4.8: M versus T

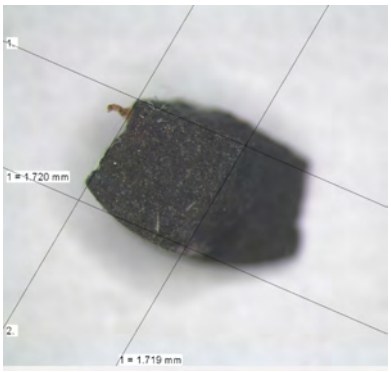

Figure 4.9: Sample photo taken by computerized Camera to measure the dimension for demagnetization factor calculation

where a, b,and c ellipsoid axes.

We found that incorporating the diamagnetic factor leads a more negative volume susceptibility. But the shape of the plot formed by row experimental data is similar. We usually compare the slope of a cooled sample below Tc, $M/H = -1$ (SI) $= -1/4\pi$(cgs), for the case in which N_d = 0.

4.4 Conclusion

The magnetization measurement was done in the temperature range 1.8-40k applying 10Oe in zero-field-cooled (ZFC) and in field-cooled (FC) conditions. In addition we took data with in the temperature range from 1.8k to 300k in a magnetic field of 1T.

From the data we determined the superconducting critical temperature,Tc of different samples. We calculated the diamagnetic volume susceptibility to see the effect of doping on superconducting volume fractions, and we found that the value is reducing for all samples. The width of ΔT_C is increasing with Mn content, indicating that strong suppressing effect of Mn.

From the diamagnetic susceptibility data we determine the value of the superconducting critical temperature Tc. It is shown that Y doping favor Tc where as Mn doping suppressed Tc even with small amount.

Magnetization versus Temperature graph shows a magnetic and/or structural transition around 120K for all superconducting samples. This reveals that there could be a magnetic transition before the onset of superconductivity, that may be explained in different ways.

Y is a bigger atom than Mn but what we see in the lattice parameter is that Mn doping reduces the c-axis. So the increase or suppression of Tc is related to not only the atomic size but also the magnetic nature of the dopant atom. We further need to understand the effect of doping on the band structure and Fermi surface (next chapter).

Chapter 5

The study on the electronic structure of the effect of Ru at Fe site on LaFeAsO and SmFeAsO

ABSTRACT

In this chapter we report the effect of Ruthenium(Ru) substitution at iron(Fe) site in LaFeAsO and SmFeAsO alloys. We did Desity of State (DOS), Fermi Surface (FS) and a band structural calculation by Density Functional Theory (DFT) as implemented in QUANTUM ESPRESSO (QE) and FLEUR codes. Even though both holes and electrons doping reported to induce superconductivity, the result of our calculation show a change in the hole bands and not in the electron bands. This means the band filling by electrons is unchanged. This indicates that Ru substitution does not induce additional electrons. This also suggest that Ru substitution has a limited pair breaking effect.

The simulation results of the Fermi surfaces show that the gap between hole-cylinder and electron-cylinder at Ru 0.25 is large. This may indicate that Ru substitution induces strong localization at 0.25 Ru, in agreement with μ SR experimental findings for oxygen doped superconducting compound [62].

Nesting may occur on 0.50 Ru substitution where the second hole cylinder coincides in size with the first electron cylinder. This change may result in changing Superconducting and magnetic properties of the system. It could be an indication for spin fluctuation. We believe that 0.5 Ru substitution stabilizes superconductivity and higher Tc can be achieved. These observations need to be explained in terms of magnetic instability. Comparison of the Fermi surfaces for $LaFe_{1-x}Ru_xAsO_{0.89}F_{0.11}$ and $SmFe_{1-x}Ru_xAsO_{0.85}F_{0.15}$ show that the higher Tc in Sm based is due to the reduction of hole bands.

5.1 Introduction

The experimental report on $LaAsFeO_{0.89}F_{0.11}$ indicates that the effect of diamagnetic impurities, Ruthenium(Ru) substitution on Iron(Fe) is less on superconducting and on magnetic ground state of LaFeAsO [61, 62] where as paramagnetic impurities Manganese(Mn) substitutions has a stronger effect [25].

As it was mentioned in the third chapter of this dissertation that our magnetization measurement shows the different effect of Mn and Y doping. But we were not able to do other measurement to see the effect on the band structure

and on the Fermi surface of each compounds and also expensive computationally. In this chapter we are focusing on the parent compound LnFeAsO (Ln = La, Sm), which is computationally reasonable.

Why La(Sm)FeAsO? The parent compound LaFeAsO is non-magnetic at room temperature. But by doping the magnetic and superconducting properties of the compound change. A deeper understanding on the doping effect of the electronic structure of this compound can provide insight into the interplay between magnetism and Superconductivity.

Where as the parent material SmFeAsO is a semiconductor or a bad metal, similarly, by doping the magnetic and superconducting properties of the compound change. In fact Ln1111 family (with Ln a lanthanide ion) shows the highest critical temperature-Tc.

Electronic structural calculation on Ln1111 shows a significant progress in understanding the system. This system has mostly P4/nmm tetragonal structure. Ru substitution on Fe site shows different properties. In $PrFe_{1-x}Ru_xAsO$, Ru substitution reduce spin density wave (SDW)[63]. Similarly in 122 family, $Ba(Fe_{1-x}Ru_x)_2As_2$, it was reported that Ru substitution suppresses spin density wave [64]. These effects may be related to the lattice parameters of the compounds.

Lattice parameters are significant to speak about the suppression or induction of Tc. Experimental result and theoretical prediction shows that Ru substitution on Fe site clearly distort the lattice structure. For instance in $Sm(Fe_{1-x}Ru_x)As(O_{0.85}F_{0.15})$, it is shown that a-axis increases linearly with the amount of Ru where as c-axis is almost constant [65]. In the previous chapter we also showed that Mn substitution on Fe site quickly decrease c-axis(Fig. 4.6). Even though Ru is a bigger atom, the effect is different than Mn. In this work we choose Ru where the effect is less on c-axis.

It was reported that, the low temperature magnetic order of the parent compound is SDW caused by nesting properties of the Fermi surface.

Hence these and other report demands that it is necessary to look closely on the band structure and Fermi surface in order to understand the effect of substituting external atoms.

In most of the experimental results Superconductivity is induced when magnetism is reduced or disappeared. The electronics structure calculation [65]

shows that Ru substitution does not induce magnetic property. In Ru doped experiment [62], $LaFe_{1-x}Ru_xAsO_{1-y}F_y$, μSR measurements show that there is a short range magnetic ordering at certain doping level (x = 0.25). Why the mag-

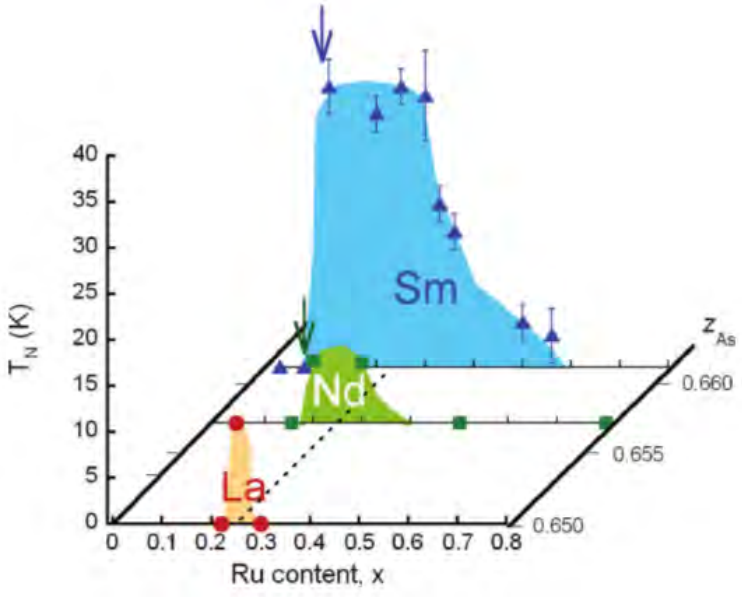

Figure 5.1: Magnetic ordering temperatures T_N from μSR measurements, taken from [62]

netic ordering temperature of the system with Sm1111 is highest at x=0.25 doping level(Fig. 5.1)? Does Ru substitution change the magnetic ordering? What does the band structure look like at this level of substitution? What about the Fermi surface? From our calculation we are trying to extract information from the band structure, DOS, and Fermi surfaces.

So far there is a limited report on the comparison of band structure and Fermi surface of Ru substitution LaFeAsO and SmFeAsO system. In this work we are reporting on the effect of Ru substitution in Fe site on LaFeAsO and SmFeAsO systems. We perform a calculation to analyze the electronic band structure, total density of state(DOS), and Fermi surface for different Ru concentration (x = 0, 0.25, 0.50, 0.75,and 1).

In general the main aim of this chapter is to examine the effect of Ru doping on electronic structure of $La(Sm)Fe_{1-x}Ru_xAsO$ within the density functional theory (DFT) calculations. We are especially interested to see the Fermi surface and band structure change under substitution, which could be correlated with superconducting temperatures of Ln1111.

5.2 Computational methods

We study the effect of variety of Ru substitution (x=0, 0.25, 0.50, 0.75, 1) on Fe site for LaFeAsO and SmFeAsO compounds. We apply first principle calculation in DFT approach with Quantum Espresso and Fleur code. We use the value of the tetragonal lattice parameter(a and c) together with internal coordinates of La and As, from Ref. [65].

The bands are plotted along the high symmetry direction in the Conventional Tetragonal-TET Brillouin zone [66] The 20x20x8 k-point mesh in the Brillouin zone was used. The DOS calculation were performed using tetrahedron method.

For 0.25 and 0.75% Ru substitution, we doubled the cell in the c-axis and we did a band folding to compare band structure in the first Brillouin zone. non spin polarized calculation were done for LaFeAsO, and spin-polarized calculations for Sm in SmFeAsO (U = 6, J = 1). We compare the result of Ru = 0 with published works.

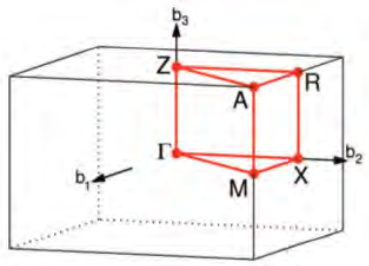

Figure 5.2: Brillouin zone of TET with path:Path: $\Gamma - X - M - \Gamma - Z - R - A - Z$

5.2.1 Quantum ESPRESSO(QE) and Fleur code

Quantum Espresso

Quantum ESPRESSO (opEn-Source Package for Research in Electronic Structure, Simulation, and optimization) contains different packages including PWscf (Plane-Wave Self-Consistent Field), Plane-Wave (PW) basis set and pseudo potentials, for the calculation of electronic-structure properties within Density-Functional Theory (DFT). QE can do Ground-state calculations, Structural Optimization, Quantum Transport, etc. The details of the code can be found from the project website[67]

Fleur

FLEUR - the FLAPW-method(Full Potential Linearized Augmented Plane Wave Method) is an all-electron method which within density functional theory is universally applicable to all atoms of the periodic table and to systems compact as well as open structures. It is widely considered to be the most precise electronic structure method in Solid State Physics [68].

We did the simulation with QE. But we encountered a convergence problem for SmFeAsO system due to lack of suitable pseudo potential in QE. Since Sm has 4f valence electron, we succeed the simulation with use FLEUR code. The result of the calculation with both codes for LaFeAsO system is quite similar.

We did a non magnetic calculation for LaFeAsO based on the μSR experimental report [62] that shows the magnetic ordering region is small compared to SmFeAsO.

5.3 Result and Discussion

5.3.1 Electronic Band structure calculation

We did a band structural calculation by Density Functional Theory(DFT) as implemented in FLEUR code and QUANTUM ESPRESSO code. We reproduced the band structure, DOS, and Fermi surface for a tetragonal lattice following the path Γ-X-M-Γ-Z-R-A-Z-(Fig. 5.2). We emphasized to check the effect of various Ru substitution(x = 0, 0.25, 0.50, 0.75, and 1) on the number, shape and size of bands.

We did a calculation for pure system that is by exchanging the atomic position (La in place of Sm and vis versa). This told us the effect of atomic position for pure system and we found that there is only a volume change.

5.3.2 Band structure

We first calculated the electronic structure of the parent compound with out Ru to compare with the already existing report. We found a good agreement. In the remaining calculation we replace for example, 50 %(0.50) Ru concentration was achieved by the substitution of two Ru out of four Fe, etc.

Since Ru has a larger atomic size than Fe, we expect a wider band and a larger

FS. Figure (5.3) and (5.4) shows the band structure of LaFeAsO and SmFeAsO for different Ru content. It is found that, the shape of the electron bands are similar for both systems LaFeAsO and SmFeAsO. There is a difference in the hole bands near Ef along Γ-Z direction for both system. But the height from Γ-Z direction for SmFeAsO is changed. It is not flat. This dispersion may result in changing the superconducting behavior of the system.
The number and size of electrons band is not changed (at M) with Ru substitution but the size of hole band is changed for both systems at the Γ- point. This may indicate that Ru substitution does not introduce additional electrons or the band filling is unchanged.
From the simulation outputs we compared the energy of each band at Γ and Z points for the hole bands and at M and X point for electron bands. The electrons band at M and X point have the same energy value for each substitution. But the energy change ΔE with respect to the Fermi level is higher for whole band than electrons band for different Ru substitutions. We also noticed that Ru changes the Fermi level E_F linearly.

5.3.3 DOS

The Density of State(DOS) for variety of Ru substitution (x=0, 0.25, 0.50, 0.75, 1) is plotted as shown in Fig (5.5) and (5.6) on the parent compound LaFeAsO and SmFeAsO.
The highest peak for all x in $LaFe_{1-x}Ru_xAsO$ and $SmFe_{1-x}Ru_xAsO$ is between -1 and 0. It is highest for x = 0.25 and lowest for x = 1.
The height of the peak is greater for SmFeAsO than LaFeAsO around -0.5. But in the other region the DOS value is higher for LaFeAsO.
We compared the total DOS of the two system for different Ru substitution. It is shown that at 0.25 and 0.75 there is an additional peak around E_F in only SmFeAsO system.
The shape is similar for all Ru substitution in LaFeAsO but in the case of SmFeAsO, it is different at x=0.25 than the rest. This could be the strong localizing effect of Ru. The effects are more pronounced for SmFeAsO system. A typical behavior at x=0.25 was shown by an experiment, where there is a static magnetic moment[62]
In the figure (Fig 5.5 and Fig 5.6), the total DOS is reduced with increasing Ru

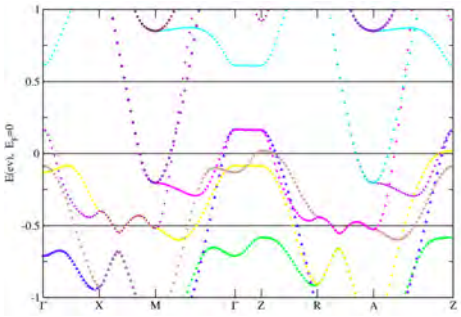

(a) x=0

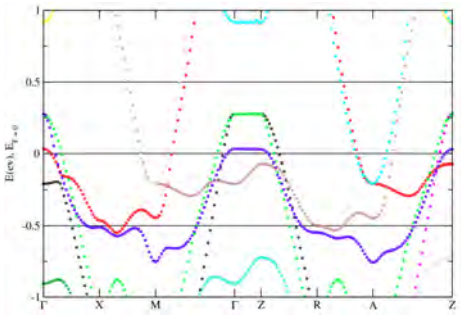

(b) x=0.50

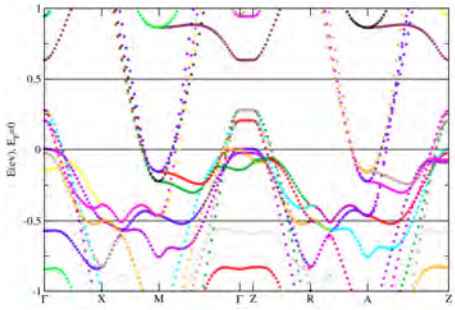

(c) x=0.25

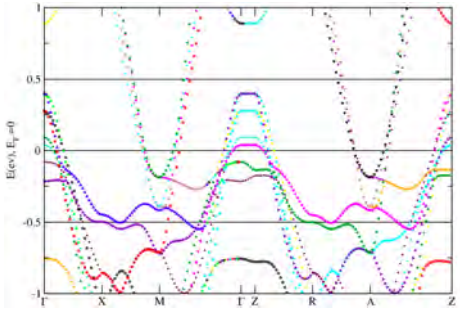

(d) x=0.75

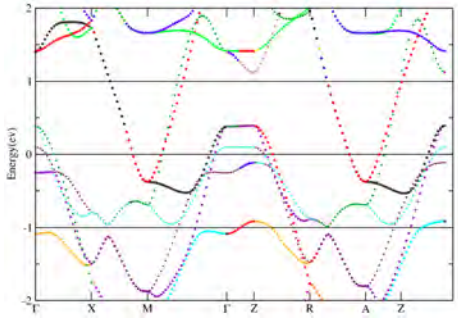

(e) x=1

Figure 5.3: Band structure for $LaFe_{1-x}Ru_xAsO$. One can clearly see the hole bands at Γ point and electron bands at X point

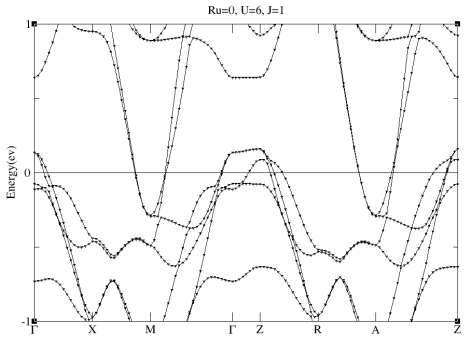

(a) x=0

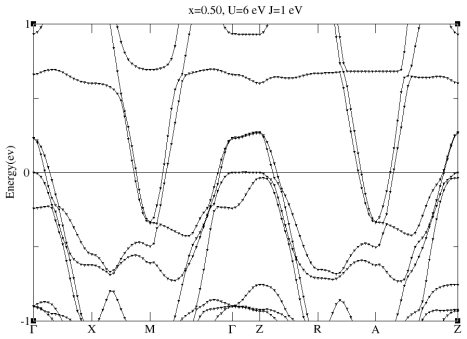

(b) x=0.50

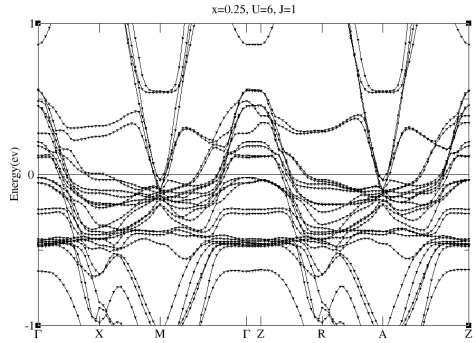

(c) x=0.25

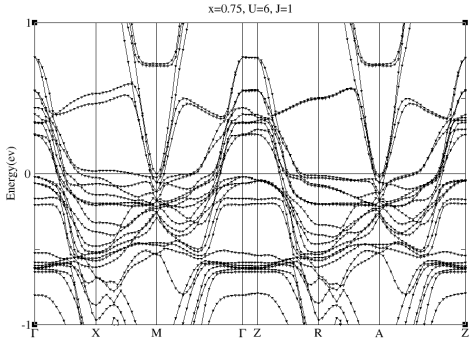

(d) x=0.75

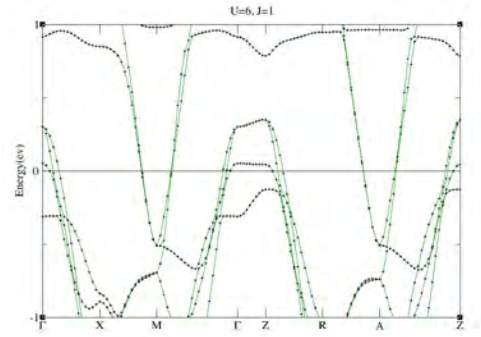

(e) x=1

Figure 5.4: Band structure for $SmFe_{1-x}Ru_xAsO$

content for both systems, comparing (x = 0, 0.50, 1). The same reduction is seen for x=0.25, and 0.75. But it has a constant value of 0.60 states/cell/ev with in 0.15 to 0.4 ev of E_F for only SmFeAsO.

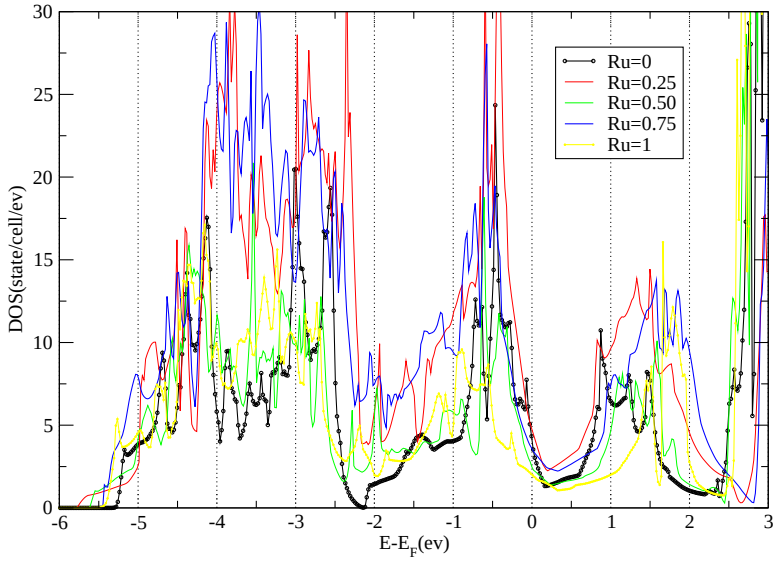

Figure 5.5: Comparison of the total DOS for La1111(the Fermi level E_F is at zero energy)

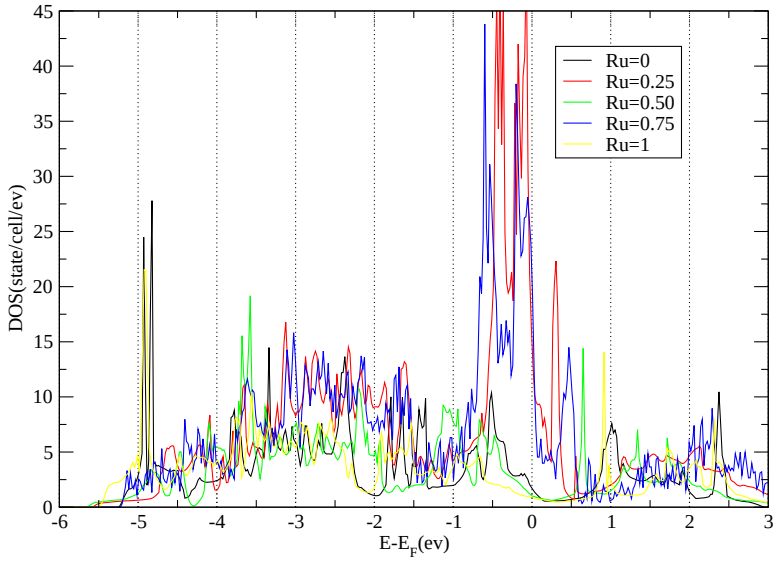

Figure 5.6: Comparison of the total DOS for Sm1111(the Fermi level E_F is at zero energy)

5.3.4 Fermi surface

In the figure (Fig 5.7 and Fig 5.8) we present the Fermi surface of La(Sm)FeAsO systems at Ru = 0 and, Ru = 0.50. From the figure of the band structure we

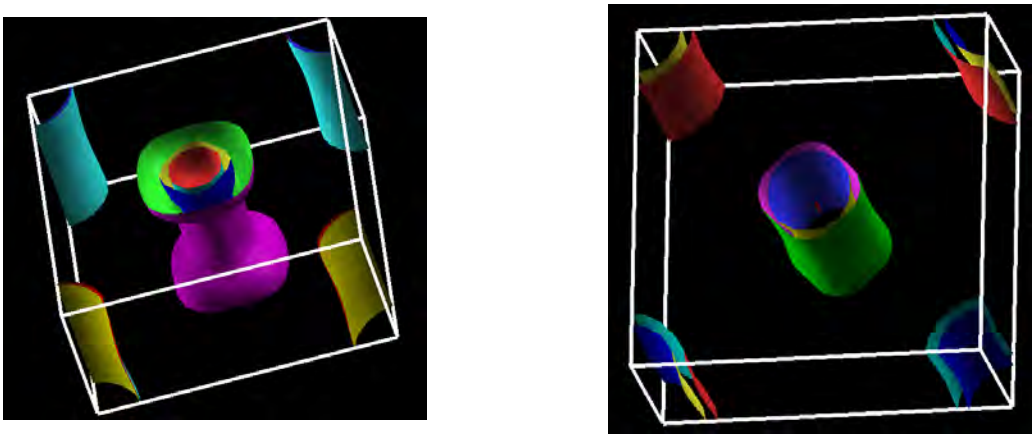

(a) x=0

(b) x=0.50

Figure 5.7: Fermi surface for $SmFe_{1-x}Ru_xAsO$, x=0, and x=0.50

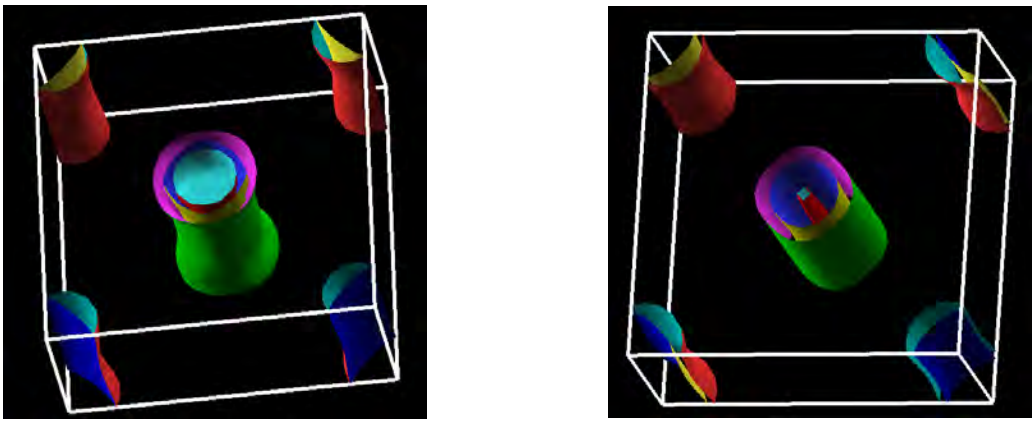

(a) x = 0

(b) x = 0.50

Figure 5.8: Fermi surface for $LaFe_{1-x}Ru_xAsO$, x = 0, and x = 0.50

can see that there are bands that cross the Fermi level and this yields multi-sheet Fermi surfaces. The FS includes electron-like cylinders in the corners of the Brillouin zone and the hole-like cylinders along the Γ-Z line. All Fermi surfaces for electron and hole are cylinder like, that confirms the two-dimensional character of electronic states, already reported for pnictides.
We found that, as already reported for LaFeAsO, the FS includes three holes and two electron cylinders. As a result of substitution the hole cylinder is affected than the electron cylinder and it becomes small for 0.5Ru substitution. Upon substitution, the electron-like cylinders are not changed while hole-like cylinders are changed in shapes. The cylinder become more thin for SmFeAsO than LaFeAsO. This indicates the effect of Ru is more for SmFeAsO than LaFeAsO.

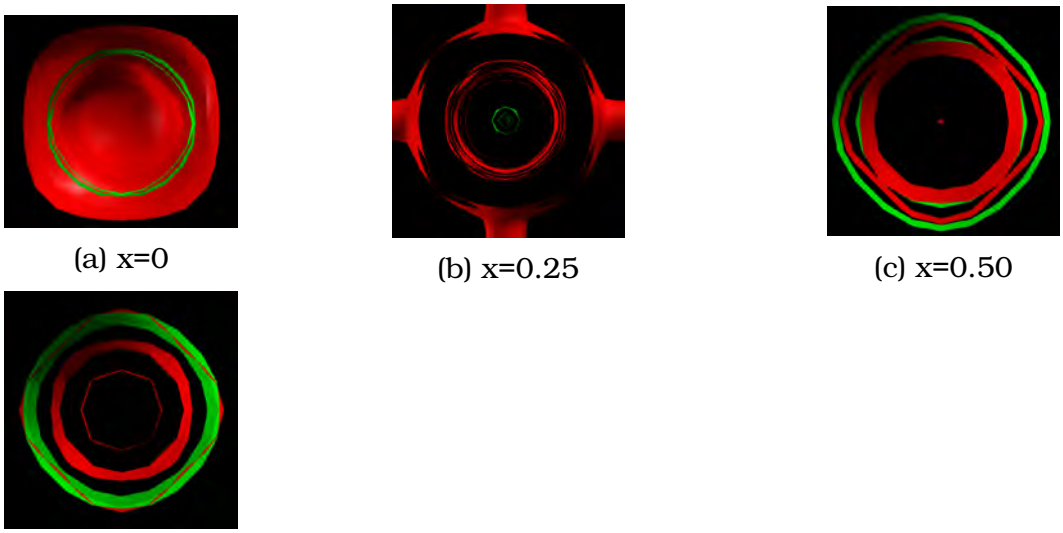

(a) x=0 (b) x=0.25 (c) x=0.50

(d) x=1

Figure 5.9: Fermi surface shifting (Nesting behavior) $SmFe_{1-x}Ru_xAsO$ (x=0, 0.25, 0.50,and 1)

We shifted the electron-like cylinders from M point to the gamma point to compare with the size of the hole cylinders(Fig. 5.9). That means to see the nesting between the electrons and holes cylinders in the parent compound. The resulting figures show that the gap between the hole and electron-like cylinders is increased except for 0.5 Ru substitution in SmFeAsO. For 0.25 substitutions the difference becomes very large. This may be the cause for inducing a static magnetic moment, which is observed by an experiment[62].
In 0.5 Ru substitution for SmFeAsO, the second hole cylinder nearly matches

with the first electron cylinder and so nesting can happen. We also observed that for over doped region where Ru=1, the last hole like cylinder is nested with electron like one. This effect may lead to nesting that may be explained in terms of SDW instability in SmFeAsO.

5.3.5 $LnFe_{1-x}Ru_xAsO_{1-y}F_y$

On the top of all we are interested to see the effect of Ru on the superconducting compound $LnFe_{1-x}Ru_xAsO_{1-y}F_y$ (y = 0.11 and y = 0.15 for Ln = La and Ln = Sm respectively). We compare the effect of Ru with the following trick. We integrate the total DOS and we get its value at the Fermi level. We add 0.11 and 0.15 (twice for double cell) per atom and we get another value. The difference is used for obtaining the Fermi surfaces.
The following figures(Fig 5.10, and Fig 5.11) are shown for comparison in the change of the Fermi surface for La and Sm based alloys. It show a disappearance of hole bands for SmFeAsO than LaFeAsO
It is clearly seen that the hole bands are disappeared or reduced for Sm based than La based. This may be the reason for the highest Tc measured Sm based alloys.

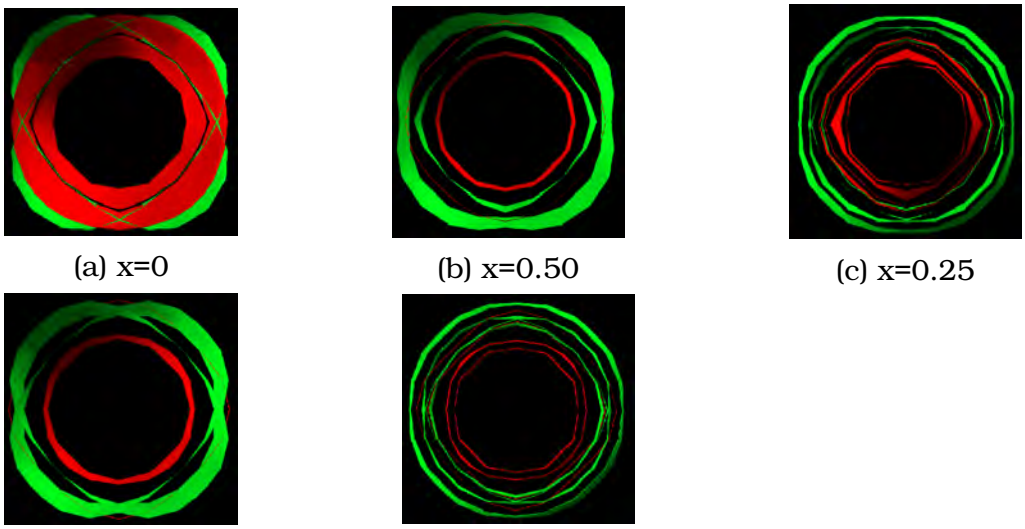

(a) x=0 (b) x=0.50 (c) x=0.25

(d) x=1 (e) x=0.75

Figure 5.10: Shifted Fermi surfaces for $LaFe_{1-x}Ru_xAsO_{0.89}F_{0.11}$

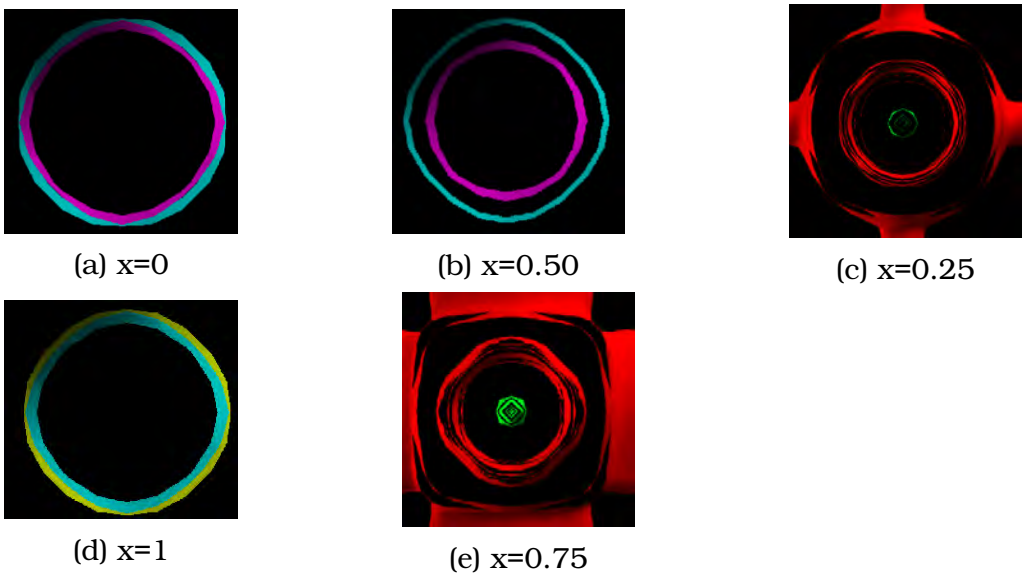

(a) x=0 (b) x=0.50 (c) x=0.25

(d) x=1 (e) x=0.75

Figure 5.11: Shifted Fermi surfaces for $SmFe_{1-x}Ru_xAsO_{0.85}F_{0.15}$

Comment on T_C

We calculated T_C based on McMillan equation(eqn. 1.3) and using the Debye temperature(θ_D = 319k) suggested in ref. [69]. We incorporate the density of state to calculate μ^*, in the equation,[ref. in [69]],

$$\mu^* = 0.13\frac{N(E_F)}{1+N(E_F)}.$$

We found that T_C = 39K for $SmFexAsO_{0.85}F_{0.15}$ when $\lambda = 2$, where the experimental value is 56K. This implies that lambda should be higher to increase T_C. So we conclude that in this system the pairing potential is very strong or the system is **strongly correlated**.

Applying the same procedure for $LaFexAsO_{0.89}F_{0.11}$, superconductivity higher Tc can be found for strong pairing potential($\lambda > 0.7$).

5.4 Conclusion

We make a calculation and simulations to obtain a band structure, DOS, and FS with QE and Fleur codes. We reproduce different shapes to see the effect of Ru substitution at Fe site around the Fermi level. Experiment show that both electron and hole doping induces Superconductivity in LaFeAsO. But here the calculation reveals that(Fig.5.3, 5.4), electrons band at M point is almost not changed, where as the hole band is changed. So we think this change in hole band is the real effect of Ru. Superconductivity in such system may not be due to addition of electrons and may not be explained by pair breaking effects. The highest peak for 0.25 Ru substitution in SmFeAsO indicates that the system is close to the magnetic instability. At this amount of substitution the gap between hole cylinder and electron cylinder is large. The larger separation observed in 0.25 Ru may dominate the localized property that may be the reason for a static magnetic ordering. This is in agreement with μSR experimental report on oxygen doped compound [62] that shows a spontaneous magnetic order at x = 1/4 for $SmFe_{1-x}Ru_xAsO_{1-y}F_y$ (y = 0.15)

The two-dimensional characteristics of the electronic states are shown from the cylindric shaped Fermi surfaces. Nesting can occur on 0.50 Ru substitution where the second hole cylinder coincides in size with the first electron cylinder. Superconductivity and the coexistence with Magnetism can occur around 0.5 Ru substitution. This may be a state for itinerant magnetic instability or a system may go away from magnetic instability in the over doped region. We predict the occurrence of coexistence between SC and M in this region between 0.25 Ru and 0.50 Ru. Comparing Fig 5.10 and Fig 5.11, which was obtained for F = 0.11 and F = 0.15, indicates that T_C is related to changes in the hole bands.

In general, Ru substitution is more sensitive for Sm based compound than for La based compound. So the enhancement of Superconductivity and the interplay with magnetism may not be explained in the same way in both LaFeAsO and SmFeAsO. On the top the effect of Ru is in changing hole bands.

Calculation for T_C indicates that superconductivity can be achieved only for a strong paring potential, which can not be explained by BCS type pairing, in agreement with experimental reports.

Bibliography

[1] Tinkham M. *Introduction to Superconductivity.* 2nd edition, McGraw Hill, Inc. United States of America, 1996.

[2] J. G. Bednorz and K. A. Muller. Possible high Tc superconductivity in the Ba-La-Cu-O systems. *Z. Phys.* B, 64,189-193 (1986).

[3] Kamihara, Y., Watanabe, T., Hirano, M. and Hosono, H., *Journal of the American Chemical Society* **130**, 3296-3297 (2008).

[4] Fengjie Ma and Zhong-Yi Lu, *Phys. Rev.* B, **78**,033111(2008).

[5] McMillan, W. L. *Phys. Rev.*, **167**, 331 (1968).

[6] Cao Wang, Linjun Li, Shun Chi, Zengwei Zhu. *EPL* **83**, 67006 (2008).

[7] Hiraku Ogino, Yutaka Matsumura, Yukari Katsura, Koichi Ushiyama, Shigeru Horii, Kohji Kishio and Jun-ichi Shimoyama, *upercond. Sci. Technol.* **22**, 075008 (2009).

[8] Shinya Sato, Hiraku Ogino1, Naoto Kawaguchi, Yukari Katsura, Kohji Kishio1, Jun-ichi Shimoyama, Hisashi Kotegawa and Hideki Tou, *Supercond. Sci. Technol* **23**, 045001 (2010).

[9] Jiangang Guo, Shifeng Jin, Gang Wang, Shunchong Wang, Kaixing Zhu, Tingting Zhou, Meng He, and Xiaolong Chen, *Phys. Rev.* B **82**, 180520(R) (2010).

[10] A. Wang, J.Ying, J.Yan, R. Liu, X.G.Luo, *Phys. Rev.* B **83**, 060512(R) (2011).

[11] Johnpierre Paglione and Richard L. Greene, *Nat Phys, advance on-line publication A. A. Kordyuk, Low teemperature physics* **38** (9), 2012.

[12] M.D. Lumsden and A.D. Christianson, *arXiv*:1004.1969 [cond-mat.supr-con], April 2010.

[13] G. R. Stewart, *Review of Modern Physics* **83**, 2011.

[14] Quantum Design, Inc., 6325 Lusk Boulevard, San Diego, CA 92121, USA.

[15] Ruebenbauer, K., ukrowski, J., Bukowski, Z., Matusiak, M. and Karpinski, *J., Acta Physica Polonica* A, **121**, 726-729 (2012).

[16] Luetkens et al., *Nature Materials* **8**, 305309 (2009).

[17] A. J. Drew, C. Niedermayer, P. J. Baker, F. L. Pratt, S. J. Blundell, T. Lancaster, R. H. Liu, G. Wu, X. H. Chen, I. Watanabe, V. K. Malik, A. Dubroka, M. Rossle, K. W. Kim, C. Baines, and C. Bernhard, *Nature Materials* **8** (4), 310314 (2009).

[18] Chu et al., Physical Review B, **79**, 014506 (2009).

[19] Vorontsov, A.B., Vavilov, M. G. and Chubukov, A.V., *Phys.Rev.* B **79**, 060508(R)(2009).

[20] L. Boeri, O. V. Dolgov, and A. A. Golubov, *Phys.Rev. Lett.* **101**, (2), 02643 (2008).

[21] A.D. Christianson, M .D. Lumsden, O. Delaire, M .B. Stone,D. L. Abernathy, M. A. McGuire, *Phys. Reiv. Lett.* **101** (15), 157004(2008).

[22] A. N. Yaresko, G.-Q. Liu, V. N. Antonov, and O. K. Andersen, *Phys. Rev.* **79**, 144421 (2009).

[23] I.I.Mazine, J. Schkalian, *Physica* C **469**, 614-627 (2009).

[24] D. J. Singh and M.-H. Du, D, *Phys.Rev. Lett.* **100**, 237003 (2008).

[25] F. Hammerath P. Bonfa S. Sanna, G. Prando, R. De Renzi, Y. Kobayashi, M. Sato, and P. Carretta, *Phys. Rev.* B **89**, 134503 (2014).

[26] F. Hammerath, M. Moroni, L. Bossoni, S. Sanna, R. Kappenberger, S. Wurmehl, A. U. B. Wolter, M. A. Afrassa, Y. Kobayashi, M. Sato, B. B Buchner and P. Carretta, *Phys. Rev.* B **92**, 020505(R) (2015).

[27] Lumsden, M.D. and Christianson, A.D., *Condensed Matter Physics* **22**, 203203 (2010).

[28] Dai, P.C., Hu, J.P. and Dagotto, E., http://arxiv.org/abs/1209.0381v1 (2012).

[29] Jun Zhao1, Q. Huang, Clarina de la Cruz1, Shiliang Li1, *Nature Materials* **7**, 953-959 (208).

[30] Jiang S, Xing H, Xuan G, Wang C, Ren Z, Feng C, Dai J, Xu Z, and Cao G., *J. Phys.: Cod. Matt.* **21**, 32203 (2009).

[31] M. A. Mcguire, D. J. Singh, A. S. Sefat, B. C. Sales, and D. Mandrus. *J. Solid State Chem.* **182**, 2326 (2009).

[32] Marianne R., Marcus T., Inga S., Falko M., Rainer P., Joachim D., Axel G., *New Journal of Physics* **11**, 025014 (2009).

[33] Blachowski, K. Ruebenbauer, J. Zukrowski, Z. Bukowski, K. Rogacki, *Phys. Rev.* B, **84**, 174503 (2011).

[34] Nandi, N.S., et al. *Phys. Rev. Lett.* **104**, 057006 (2010).

[35] K.W. Lee, Progress in Superconductivity **10**, 123-127 (2009).

[36] I.I. Mazin, M.D. Johannes, L. Boeri, K. Koepernik, and D.J. Singh, *Phys. Rev.* B **78**, 085104 (2008).

[37] Kim JS, Khim S, Yan L, Manivannan N, Liu Y, Kim I, Stewart GR, *J.Phys.: Condens. Matter* **21**, 102203 (2009).

[38] Chang-Youn Moon, Se Young Park, and Hyoung Joon Choi, *Phys. Rev.* B **80**, 054522 (2009).

[39] Qimiao Si and Elihu Abrahams, *Phys. Rev. Lett.* **101**, 076401 (2008).

[40] G.Rickayzen, Theory of superconductivity, JohnWiley and Sons,Inc.,NewYork,1965.

[41] A.S.Chakravorty. Introduction to the magnetic properties of solids, John Wiley and Sons, Inc.,NewYork,1980.

[42] BOGOLIUBOV N. N. AND TYABLIKOV S. V.: Doklady Acad. Nauk SSSR, 53:126, 1959.

[43] TYABLIKOV S. V.: Methods in the Quantum Theory of Magnetism (Plenum Press, New York) 1967.

[44] William, D.B. Fundamentals of Many-Body Physics Principles and Methods. *Springer-Verlag Berlin Heidel-berg* 2009.

[45] Han F, Zhu X, Cheng P, *Phys. Rev.* B **80**, 024506 (2009).

[46] Chen, H., et al, *Europhysics Letters* **85**, 17006 (2009).

[47] Hai-Hu Wen, Gang Mu, Lei Fang, Huan Yang and Xiyu Zhu, *Euro physics Letters* **82** (1), 17009 (2008).

[48] Karolina Kasperkiewicz, Jan-Willem G. Bos, Andrew N. Fitch, Kosmas Prassides, and Serena Margadonna. arXiv:cond-mat/0809.1755.

[49] Takahashi H1, Igawa K, Arii K, Kamihara Y, Hirano M, Hosono H. *Nature* **453**, 376 (2008).

[50] Zhi-An Ren, Guang-Can Che, Xiao-Li Dong, Jie Yang, Wei Lu, Wei Yi, Xiao-Li Shen, Zheng-Cai Li, Li-Ling Sun, Fang Zhou, Zhong-Xian Zhao, *Euro phys. Lett.* **83**, 17002 (2008)a.

[51] Cao Wang, et al, *J. Phys. Condens. Matter* **21**, 142203 (2008).

[52] Peng Cheng,et al, *Euro physics Letters* **85**, 67003

[53] A.Thaler et al, *Phys. Rev.* B **84**, 144528.

[54] Y. Texier et al., *Euro phys. Lett.* **99**, 17002 (2012).

[55] J. Li,et al, *Phys. Rev.* **85**, 214509 (2012).

[56] P.M. Shirage, K. Miyazawa, H. Kito, H. Eisaki and A. Iyo, *Phys. Rev.* B **78**, 172503 (2008).

[57] Masatoshi SATO, *Journal of the physical society of Japan* **79**, 1(2010).

[58] C.H.Lee, et al., *J.Phys. Soc. Jpn.* **77**, 083704 (2008).

[59] M. Sato, Y. Kobayashi, S. C. Lee, H. Takayashi, E. Satomi, and Y. Miura, *J. Phys. Soc. Jpn.* **79**, 014710 (2010).

[60] J. A. Osborn.Diamagnetizing Factors of the General Ellipsoid. *Phys. Rev.* **67**, 351 (1945).

[61] S.Sanna, P. Carretta, P. Bonfa, G. Prando, G. Allodi. *Phys. Rev. Lett.* **107**, 227003 (2011).

[62] S. Sanna, P.Carretta, R.De Renzi, G.Prando, P.Bonfa, M.Mazzani, G.Lamura, *Phys. Rev.* B **87**, 134518 (2013).

[63] M. A. McGuire, D. J. Singh, A. S. Sefat, B. C. Sales, and D. Mandrus, *J. Solid State Chem.* **182**, 2326 (2009).

[64] Lijiun Zhang and D. J. Singh, *Phys. Rev.* **79**, 174530 (2009).

[65] M. Tropeano, M.R. Cimberle, C. Ferdeghini, G.Lamura, A. Martinelli, A. Palenzona, I. Pallecchi, A. Sala, I.Sheikin, F. Bernardini, M. Monni, S. Massidda, and M. Putti 1,2, *Phys. Rev.* **81**, 184504 (2010).

[66] Wahyu Setyawan, Stefano Curtarolo. *Computational Materials Science* **49**, 299-312 (2010).

[67] P. Giannozzi et al., *J.Phys.:Condens. Matter* **21**, 395502 (2009).
Quantum Espresso: URL http://www.quantum-espresso.org"

[68] Fleur: http://wwww.flapw.de..

[69] Alexander P.Koufos, Dimitros A. Papaconstantopoulos, and Michael J. Mwhl, *Phys. Rev* B **89**, 035150 (2014).

PUBLICATION

1. F. Hammerath, M. Moroni, L. Bossoni, S. Sanna, R. Kappenberger, S. Wurmehl, A. U. B. Wolter, **M. A. Afrassa**, Y. Kobayashi, M. Sato, B. B Buchner and P. Carretta, *Phys. Rev.* B **92**, 020505(R) (2015).

2. Mesfin A. **Afrassa**, Poran Singh, World Journal of Condensed Matter Physics, 4, 53-57(2014).

3. M. Moroni, S. Sanna,G. Lamura, T. Shiroka, R. Kappenberger, S. Wurmehl, A.U.B. Wolter, **M. A. Afrassa**, B. Buchner, and P. Carretta.
(arXiv:1605.09334v1 [cond.math.supr.con] 30 May 2016)

4. **M. A. Afrassa**, P.Singh, The study on the effect of Ruthenium(Ru) in LaFeAsO (communicated).

Seminar and conference participation

1. Workshop on NMR, μSR, Mossbauer Spectroscopies in the study of iron based and other unconventional high Tc superconductors, 17-18 July 2014, Dresden, Germany.
2. Workshop on critical row element substitutions in electronic and optoelectronic technologies(REST), 9-10 April 2015, Cagliari, Italy.

Declaration

I hereby declare that this PhD dissertation is my original work, has not been presented for a degree in any other University and that all the sources of material used for the dissertation have been dully acknowledged.

Name: Mesfin Asfaw

Signature: _____

This PhD dissertation has been submitted for examination with my approval as University advisor.

Name: prof. P. Singh

Signature: _____

Place and date of submission:
Addis Ababa University
Department of Physics
April 2016